Chemistry in Cages: Zeolite-Entrapped Hexairidium Cluster Catalysts

S. Kawi, J.-R. Chang, and B. C. Gates*

Contribution from the Center for Catalytic Science and Technology, Department of Chemical Engineering, University of Delaware, Newark, Delaware 19716

Received August 5, 1992. Revised Manuscript Received October 30, 1992

Abstract: Iridium carbonyl clusters in the cages of NaY zeolite were prepared from adsorbed $[Ir(CO)_2(acac)]$. Reductive carbonylation of this precursor in CO at 1 atm and 50 °C gave $[Ir_4(CO)_{12}]$, which was converted in CO at 125 °C and 1 atm to the isomer of $[Ir_6(CO)_{16}]$ with edge-bridging ligands and in CO + H_2 at 250 °C and 20 atm to the isomer of $[Ir_6(CO)_{16}]$ with face-bridging ligands, both identified by infrared and extended X-ray absorption fine structure (EXAFS) spectra. The zeolite containing the latter catalyzed the CO hydrogenation reaction at 20 atm and 250 °C, giving a high selectivity to propane and being stable for a number of days in a flow reactor. Either isomer of $[Ir_6(CO)_{16}]$ in the zeolite could be decarbonylated in H_2 at 300 °C and 1 atm and recarbonylated to give either isomer of $[Ir_6(CO)_{16}]$. The decarbonylated cluster in the presence of H_2 is inferred from EXAFS spectra to be predominantly Ir_6 with an octahedral structure and an average Ir–Ir bond distance of 2.71 Å. These results illustrate the potential for preparation of supported metal clusters with controlled nuclearities and open the door to precise characterization of the structures and properties of uniform, highly dispersed supported metal catalysts.

Introduction

Nanostructures dispersed in the molecular-scale cages of crystalline aluminosilicates (zeolites) include metal[1-3] and metal carbonyl clusters,[4-8] metal oxides,[9,10] and metal sulfides.[11,12] The encaged metal carbonyl clusters are catalysts with unusual selectivities for CO hydrogenation[6,13-17] and potential shape-selective catalysts.[18] The encaged metal oxides[9,10] and metal sulfides[11,12] are potential semiconductors that offer novel electronic and optical properties. The preparation of unique—nearly molecular—encaged nanostructures is often difficult, as mixtures often form, not only inside the cages but also outside the zeolite crystallites. To develop the chemistry in zeolite cages, it is essential to synthesize the encaged structures in high yields and to characterize them precisely; extended X-ray absorption fine structure (EXAFS) spectroscopy is well-suited to these materials, but so far there are only a few characterizations of them that include thorough EXAFS analyses.[19-21]

The samples chosen for this research are hexairidium clusters in zeolite NaY; preliminary infrared results[3] indicate that $[Ir_6(CO)_{16}]$ and decarbonylated clusters, suggested to be Ir_6, have been formed in the zeolite supercages. Here we report the synthesis, characterization by infrared and EXAFS spectroscopies, and catalytic properties of the zeolite containing $[Ir_6(CO)_{16}]$; we also report evidence that the cluster nuclearity of six is retained in the reversible decarbonylation and carbonylation of the encaged clusters.

Results

Reactivity of $[Ir(CO)_2(acac)]$ in NaY Zeolite under CO at 1 atm. $[Ir(CO)_2(acac)]$ was adsorbed by NaY zeolite from hexane solution. Uptake of the organometallic species by the zeolite required some hours and was not complete even after 2 days of contacting. The infrared spectrum of the supernatant solution showed that some $[Ir(CO)_2(acac)]$ was still present, and there was no evidence of other metal carbonyls.

Upon removal of the solvent from the black $[Ir(CO)_2(acac)]$-containing zeolite by evacuation, the solid became pale yellow. Reintroduction of the solvent gave a brown material, which became pale yellow again upon evacuation. The infrared spectrum of the pale yellow solid (Figure 1A) has two strong carbonyl bands, at 2080 and 2000 cm^{-1}, indicating the existence of an iridium dicarbonyl species.

A sample of the $[Ir(CO)_2(acac)]$-containing zeolite in an infrared cell was exposed to flowing CO at 40 °C. After about 6 h, the spectrum (ν_{CO}: 2114 w, 2070 s, 2029 m, sh cm^{-1}) (Figure 1B) closely resembled that of $[Ir_4(CO)_{12}]$ in tetrahydrofuran (THF) solution (ν_{CO}: 2110 vw, 2068 vs, 2028 m, sh cm^{-1}). The solid sample was light yellow, the color of $[Ir_4(CO)_{12}]$. EXAFS data[21] are consistent with the identification of $[Ir_4(CO)_{12}]$.

When the temperature was increased to 125 °C, a bridging carbonyl band appeared at 1816 cm^{-1} and increased in intensity as the terminal carbonyl bands shifted to higher frequencies. The spectrum attained a steady state after 4 h at 125 °C (Figure 1C); the sample was light yellow.[3] The spectrum is almost the same as the THF solution spectrum of the isomer of $[Ir_6(CO)_{16}]$ that has four edge-bridging and terminal ligands,[22] except that the

* Address correspondence to this author at the Department of Chemical Engineering, University of California, Davis, CA 95616.

(1) Jacobs, P. A. In *Metal Clusters in Catalysis*; Gates, B. C., Guczi, L., Knözinger, H., Eds.; Elsevier: Amsterdam, 1986; p 357.
(2) Kawi, S.; Gates, B. C. *Catal. Lett.* **1991**, *10*, 263.
(3) Kawi, S.; Gates, B. C. *J. Chem. Soc., Chem. Commun.* **1991**, 994.
(4) Rode, E. J.; Davis, M. E.; Hanson, B. E. *J. Catal.* **1985**, *96*, 574.
(5) Sheu, L.-L.; Knözinger, H.; Sachtler, W. M. H. *J. Am. Chem. Soc.* **1989**, *111*, 8125.
(6) Kawi, S.; Gates, B. C. *J. Chem. Soc., Chem. Commun.* **1992**, 702.
(7) Bergeret, G.; Gallezot, P.; Lefebvre, F. *Stud. Surf. Sci. Catal.* **1986**, *28*, 401.
(8) Bergeret, G.; Gallezot, P.; Gelin, P.; Ben Taarit, Y.; Lefebvre, F.; Naccache, C.; Shannon, R. D. *J. Catal.* **1987**, *104*, 279.
(9) Ozin, G. A.; Ozkar, S.; Moller, K.; Bein, T. *J. Am. Chem. Soc.* **1990**, *112*, 9575.
(10) Ozin, G. A.; Malek, A.; Prokopowicz, R.; Macdonald, P. M.; Ozkar, S.; Moller, K.; Bein, T. *Mater. Res. Soc. Symp. Proc.* **1991**, *233*, 109.
(11) Herron, N.; Wang, Y.; Eddy, M. M.; Stucky, G. D.; Cox, D. E.; Moller, K.; Bein, T. *J. Am. Chem. Soc.* **1989**, *111*, 530.
(12) Moller, K.; Eddy, M. M.; Stucky, G. D.; Herron, N.; Bein, T. *J. Am. Chem. Soc.* **1989**, *111*, 2564.
(13) Zhou, P.-L.; Gates, B. C. *J. Chem. Soc., Chem. Commun.* **1989**, 347.
(14) Zhou, P.-L.; Maloney, S. D.; Gates, B. C. *J. Catal.* **1991**, *129*, 315.
(15) Lee, T. J.; Gates, B. C. *Catal. Lett.* **1991**, *8*, 15.
(16) Kawi, S.; Chang, J.-R.; Gates, B. C. *J. Catal.*, in press.
(17) Fraenkel, D.; Gates, B. C. *J. Am. Chem. Soc.* **1980**, *102*, 2478.
(18) Mantovani, E.; Palladino, N.; Zanobi, A. *J. Mol. Catal.* **1977**, *3*, 285.
(19) Maloney, S.; Zhou, P.-L.; Kelley, M. J.; Gates, B. C. *J. Phys. Chem.* **1991**, *95*, 5409.
(20) Moller, K.; Koningsberger, D. C.; Bein, T. *J. Phys. Chem.* **1989**, *93*, 6116.
(21) Kawi, S.; Chang, J.-R.; Gates, B. C., to be published.

0002-7863/93/1515-4830$04.00/0

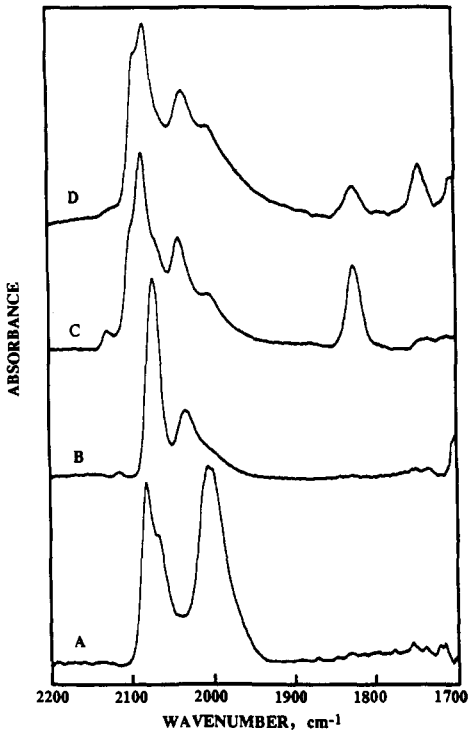

Figure 1. Infrared spectra taken during treatment of the initially prepared sample made from $[Ir(CO)_2(acac)]$ and NaY zeolite: (A) $[Ir(CO)_2(acac)]$ adsorbed in NaY zeolite; (B) after treatment in CO at 40 °C for 6 h; (C) after additional treatment in CO at 125 °C for 4 h; and (D) after additional treatment in CO at 175 °C for 1 h.

frequencies of the terminal CO bands of the encaged cluster are shifted to higher frequencies and that of the bridging ligand is shifted to a lower frequency. Thus the iridium carbonyl is tentatively assigned as $[Ir_6(CO)_{16}]$ with edge-bridging carbonyl ligands. A similar infrared spectrum has been observed for an iridium carbonyl in a zeolite and assigned incorrectly as $[Ir_4(CO)_{12}]$,[23] but this report appeared prior to the identification of the isomer of $[Ir_6(CO)_{16}]$ with edge bridging CO ligands.

With the sample still in the cell under CO at 1 atm, the temperature was raised to 175 °C. After 1 h at 175 °C, the band at 1816 cm^{-1} decreased slightly in intensity, the terminal carbonyl peaks shifted about 10 cm^{-1} to higher frequencies, and a peak appeared at 1730 cm^{-1} (Figure 1D); the sample was still light yellow. The 1730-cm^{-1} band is characteristic of the isomer of $[Ir_6(CO)_{16}]$ that has four face-bridging and 12 terminal ligands.[24,25] The spectra show that roughly 60% of the zeolite-encaged $[Ir_6(CO)_{16}]$ with edge-bridging ligands had been converted to $[Ir_6(CO)_{16}]$ with face-bridging ligands. At temperatures greater than 240 °C, the infrared bands of the carbonyl species were broadened, and after >5 h at 250 °C, the infrared spectrum showed a broad band at 2030 cm^{-1} characteristic of CO chemisorbed on iridium metal;[26] the sample was then gray, and the metal had evidently aggregated outside the zeolite pores.

Attempts to extract iridium carbonyls from samples containing either of the two $[Ir_6(CO)_{16}]$ isomers with THF or with bis(triphenylphosphine)iminium chloride, [PPN][Cl], in THF were unsuccessful. The supernatant solutions remained colorless and had no carbonyl absorptions, consistent with the stable entrapment of the clusters in the zeolite.

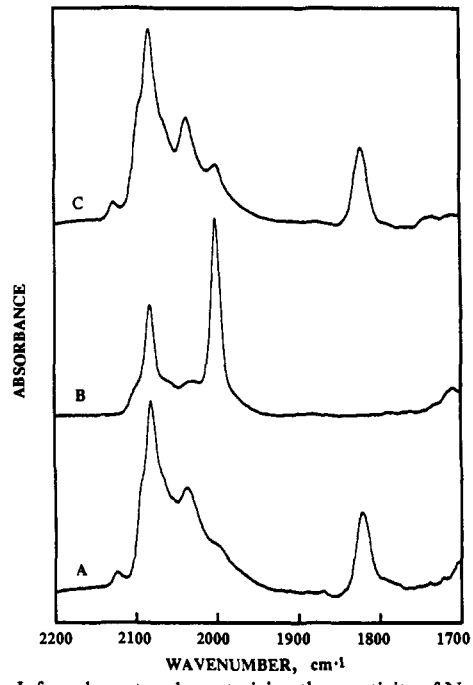

Figure 2. Infrared spectra characterizing the reactivity of NaY zeolite-supported $[Ir_6(CO)_{16}]$ with edge-bridging ligands in O_2 at 125 °C: (A) NaY zeolite-supported $[Ir_6(CO)_{16}]$ with edge-bridging ligands; (B) after treatment in flowing He/O_2 at 125 °C for 15 min; and (C) after subsequent CO treatment at 125 °C for 30 min.

Reactivity of Zeolite-Supported Iridium Carbonyl Clusters in O_2 and in Air. A sample prepared from $[Ir(CO)_2(acac)]$ in NaY zeolite was treated in the infrared cell in flowing CO at 125 °C for 12 h to form the isomer of $[Ir_6(CO)_{16}]$ with edge-bridging ligands (Figure 2A). The CO stream was then replaced by a stream of He containing 2% O_2. The infrared spectrum immediately changed; the bands at 2085 and 1816 cm^{-1} decreased and the bands at 2080 and 2000 cm^{-1} increased in intensity. After about 15 min, the bands at 2085 and 1816 cm^{-1} had disappeared, leaving two intense bands in the ν_{CO} region (Figure 2B), indicative of the oxidized sample. When this sample was treated in flowing CO at 125 °C, the spectrum of the isomer of $[Ir_6(CO)_{16}]$ with edge-bridging ligands reappeared (Figure 2C).

Another sample prepared from $[Ir(CO)_2(acac)]$ and NaY zeolite was treated in the infrared cell in flowing CO at 125 °C for 12 h to form the isomer of $[Ir_6(CO)_{16}]$ with edge-bridging ligands (Figure 3A). The sample was cooled to room temperature in flowing CO. The cell was then purged with N_2 for 15 min to remove CO gas. The spectrum of $[Ir_6(CO)_{16}]$ was maintained. The sample was then exposed to air. The bridging band at 1816 cm^{-1} decreased in intensity, and the terminal bands shifted to lower frequencies after the sample was exposed to air for 5 min (Figure 3B). After the sample was exposed to air for 15 min, its infrared spectrum was similar to that of $[Ir_4(CO)_{12}]$ (Figure 3C). The isomer of $[Ir_6(CO)_{16}]$ with edge-bridging ligands was reformed by treatment of the sample in flowing CO at 125 °C for 30 min (Figure 3D).

Catalytic CO Hydrogenation. All the Ir-containing samples were found to catalyze CO hydrogenation at temperatures of 225–275 °C. Conversions were measured as a function of time on stream in a flow reactor. Catalytic activities are represented by rates of reaction calculated from low-conversion data and are expressed in units of [mol of CO converted to hydrocarbons (mol of total Ir·s)$^{-1}$]. All the experiments reported here were conducted with CO conversions between 0.1 and 2.0%. The standard conditions were chosen to be 250 °C, 20 atm, space velocity = 20 mL (NTP) (g of catalyst·min)$^{-1}$, and CO/H_2 feed molar ratio = 1. In a blank test with the reactor packed with NaY zeolite, no hydrocarbon formation was observed.

(22) Garlaschelli, L.; Martinengo, S.; Bellon, P. L.; Demartin, F.; Manassero, M.; Chiang, M. Y.; Wei, C.-Y.; Bau, R. *J. Am. Chem. Soc.* **1984**, *106*, 6664.
(23) Gelin, G.; Ben Taarit, Y.; Naccache, C. *Proc. 7th Int. Congr. Catal. (Tokyo)* **1980**, *B*, 898.
(24) Malatesta, L.; Caglio, G.; Angoletta, M. *Chem. Commun.* **1970**, 532.
(25) Angoletta, M.; Malatesta, L.; Caglio, G. *J. Organomet. Chem.* **1975**, *94*, 99.
(26) McVicker, G. B.; Baker, R. T. K.; Garten, R. L.; Kugler, E. L. *J. Catal.* **1980**, *65*, 207.

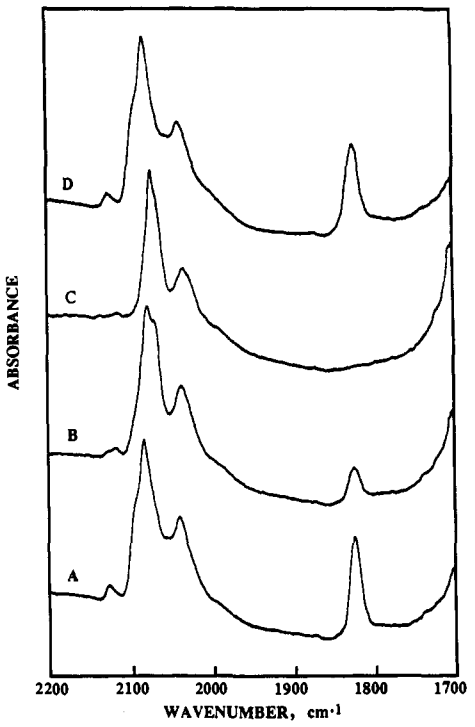

Figure 3. Infrared spectra characterizing the reactivity of NaY zeolite-supported $[Ir_6(CO)_{16}]$ with edge-bridging ligands in air at 25 °C: (A) NaY zeolite-supported $[Ir_6(CO)_{16}]$ with edge-bridging ligands; (B) after exposure to air at 25 °C for 5 min; (C) after exposure to air at 25 °C for 15 min; and (D) after subsequent treatment in CO at 125 °C for 30 min.

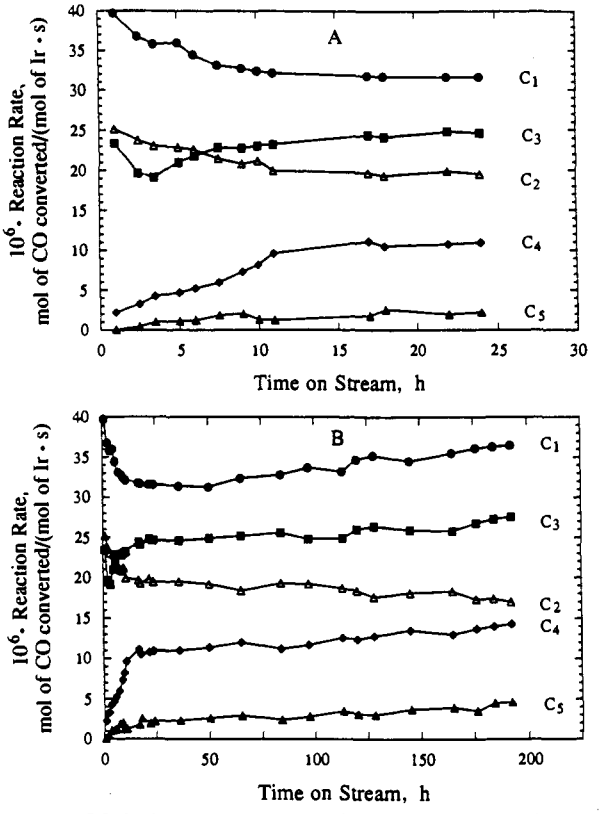

Figure 4. CO hydrogenation catalyzed by zeolite-supported iridium carbonyl clusters: dependence of product distribution on time on stream in a flow reactor up to (A) 1 day and (B) 8 days. Reaction conditions: 250 °C, 20 atm, CO/H_2 = 1.0 (molar).

Typical product distributions with the zeolite-supported Ir catalyst, which was prepared from the adsorbed $[Ir(CO)_2(acac)]$ in NaY zeolite, on stream for 1 day and 8 days are shown in parts A and B of Figure 4, respectively. The catalyst gave relatively high yields of C_2–C_4 hydrocarbons, predominantly alkanes. Products with >5 carbon atoms were formed in only very low yields at the low conversions observed (≈0.3%). The catalyst showed major changes in product distribution during the first 12 h on stream; most notable was the increased rate of formation of products with more than 3 carbon atoms relative to those with 1 or 2 carbon atoms. After 12 h on stream, the selectivity changed only slightly.

The catalysts that had been on stream for 1 day and 8 days were removed from the reactor in the absence of air; they were yellow, with no visible indication of metallic iridium.

The hydrocarbon product distributions after 1 day and after 8 days on stream were approximately the same, as shown in the Schulz–Flory plots of Figure 5, A and B, respectively. Substantial deviations from linear Schulz–Flory plots are evident, with maxima at C_3.

The good stability of the zeolite-supported catalyst provided an opportunity for investigation of the kinetics of CO hydrogenation. The effects of space velocity, pressure, and feed composition on catalyst performance were investigated under steady-state conditions. The conversion to hydrocarbons was observed to be proportional to the inverse space velocity, confirming that the conversions were differential and determined reaction rates directly.

High pressures of $CO + H_2$ (about 20 atm) were found to be necessary for maintaining stable catalyst performance. At lower pressures, the catalyst deactivated slowly in operation. After 24 h in operation at 1 atm and otherwise the same conditions stated above, the used catalyst removed from the reactor was dark gray, consistent with the formation of iridium metal particles on the outer zeolite surface. The product distribution observed with the deactivated catalyst was different from those stated above. The yields of methane and ethane were higher; these product distributions are characteristic of the linear Schulz–Flory plots observed for conventional supported metal catalysts.

To determine the effect of high H_2 partial pressures on catalyst stability, a sample of $[Ir(CO)_2(acac)]$-containing zeolite was treated for 24 h at 250 °C and 20 atm in flowing CO/H_2 with a molar ratio of 1/3. The activity of this catalyst increased during operation in the flow reactor. The activity of the catalyst after 24 h on stream was about 7 times higher than that observed for the catalyst used in equimolar $CO + H_2$. When the former catalyst sample was removed from the reactor, the upstream end of the catalyst bed was black, consistent with the conclusion that iridium metal particles had formed on the zeolite outer surface after treatment at the relatively high H_2 partial pressure. The iridium metal is evidently more active catalytically than the encaged species that had been present in the zeolite.

Catalyst Characterization by Infrared Spectroscopy. A sample of catalyst, which was prepared from the adsorbed $[Ir(CO)_2(acac)]$ in NaY zeolite and had been used in CO hydrogenation with an equimolar $CO + H_2$ feed, was removed from the reactor after 1 day on stream and characterized by infrared spectroscopy. Another sample was used for 8 days and then removed from the reactor and characterized. Both samples catalyzed CO hydrogenation at 20 atm and 250 °C with a feed of equimolar $CO + H_2$; the two samples exhibited equivalent catalyst performance (Figures 4 and 5). After removal from the reactor, each catalyst sample was yellow (suggesting the presence of iridium carbonyl species); there was no visual indication of metallic species.

The infrared spectra of these two used catalysts are shown in Figure 6, A and B, respectively. The spectra of the two samples are virtually the same, and the spectra in the ν_{CO} region are almost the same as the spectrum of the isomer of $[Ir_6(CO)_{16}]$ (in THF solution) that has four face-bridging ligands,[24,25] except that the frequencies of the terminal CO bands of the encaged cluster are shifted to higher frequencies and that of the bridging ligand is

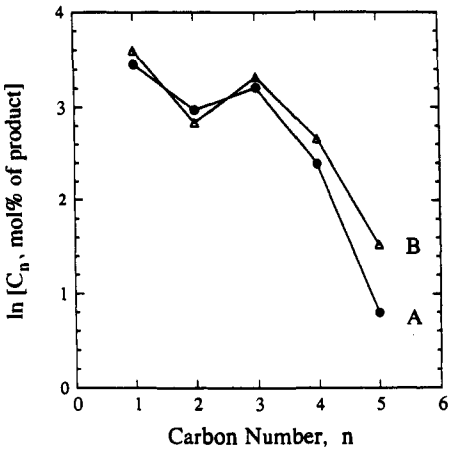

Figure 5. Hydrocarbon product distributions in CO hydrogenation catalyzed by zeolite-supported iridium carbonyl clusters: (A) 1 day on stream and (B) 8 days on stream.

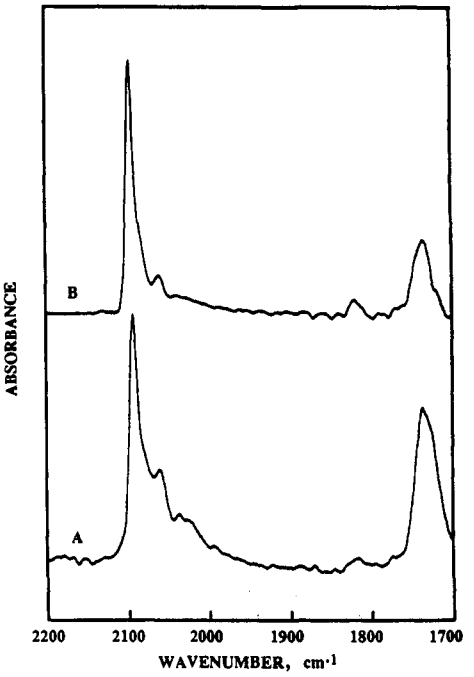

Figure 6. Infrared spectra in the ν_{CO} stretching region of used CO hydrogenation catalysts after exposure to equimolar CO + H_2 at 20 atm and 250 °C for (A) 1 day and (B) 8 days.

shifted to a lower frequency relative to those of the cluster in solution. These results suggest that the predominant form of the iridium in the catalyst samples was the isomer of $[Ir_6(CO)_{16}]$ with face-bridging ligands, which was stable under reaction conditions.

Attempts to extract iridium carbonyls from the two used catalyst samples with THF or with [PPN][Cl] in THF were unsuccessful. The supernatant solutions remained colorless and had no carbonyl absorptions, consistent with the stable entrapment of the carbonyl clusters in the zeolite.

Catalyst Characterization by EXAFS Spectroscopy. The two used catalyst samples were also characterized by EXAFS spectroscopy. The normalized EXAFS function for each sample was obtained from the average of the X-ray absorption spectra from two scans by a cubic spline background subtraction. The EXAFS function was normalized by division by the height of the absorption edge.

The raw EXAFS data characterizing the catalyst that had been on stream for 1 day (Figure 7A) show oscillations up to a value of k, the wave vector, of about 14 Å^{-1}, indicating the presence of near-neighbor high-Z backscatterers, which are inferred to be Ir. Since the infrared data indicate that carbonyl ligands were also present in the sample, the data were first analyzed for Ir–Ir, Ir–C, and Ir–O* interactions (where O* refers to carbonyl oxygen). The EXAFS analysis was done with experimentally determined reference files that are described in the section entitled EXAFS Reference Data. The raw EXAFS data characterizing the 1-day sample were Fourier transformed with a k^2 weighting over the range $3.52 < k < 14.35$ Å^{-1} with no phase correction. The Fourier-transformed data were then inverse transformed in the range $0.40 < r < 3.35$ Å (where r is the distance from the absorber Ir atom) to isolate the major contributions from low-frequency noise and higher-shell contributions.

With the Koningsberger difference file technique,[27,28] the Ir–Ir contribution, the largest in the EXAFS spectrum, was then estimated. Since the Ir–O* contribution was found to be strongly coupled with the Ir–Ir contribution, these two contributions had to be analyzed simultaneously. The structural parameters were estimated initially by fitting the data in the high-k range ($7.5 < k < 14.0$ Å^{-1}). The multiple scattering associated with Ir–C–O* groups was found to be significant, with Ir–support and Ir–C contributions being insignificant in this range. Further analysis, following the subtraction of the calculated Ir–Ir and Ir–O* contributions from the raw data, led to characterization of the Ir–C_t and Ir–C_b contributions (where the subscripts t and b refer to terminal and bridging, respectively). The fit of the raw data with the sum of the four contributions was still not satisfactory, and it was inferred that another contribution had to be accounted for. The fifth contribution involved another low-atomic-number backscatterer, which was assumed to be the oxygen of the zeolite, referred to as Ir–$O_{support}$. The structural parameters characterizing the Ir–C_t, Ir–C_b, and Ir–$O_{support}$ contributions were determined by fitting the residual spectrum. The initial guesses for parameter estimation were obtained by adjusting the coordination parameters to give the best fit of the residual spectrum in r space. The calculated Ir–C and Ir–$O_{support}$ contributions were then subtracted from the raw data. Better parameters for the Ir–Ir and Ir–O* contributions were then estimated by fitting the residual spectrum. The iteration was continued until good overall agreement was obtained.

The parameters determined in this fitting routine are summarized in Table I, and the comparisons of the data and the fit, both in k space and in r space, are shown in Figure 7B–D. The residual spectrum determined by subtracting the Ir–Ir + Ir–$O_{support}$ contributions from the EXAFS data (which gives evidence of the carbonyl ligands) is shown in Figure 7E.

The number of parameters used to fit the data in this main-shell analysis is 20; the statistically justified number is approximately 21, estimated from the Nyquist theorem,[29] $n = (2\Delta k \Delta r/\pi) + 1$, where Δk and Δr respectively are the k and r ranges used in the forward and inverse Fourier transforms ($\Delta k = 10.83$ Å^{-1}; $\Delta r = 2.95$ Å).

The EXAFS data characterizing the catalyst sample that had been used 8 days in the flow reactor were analyzed in the same way. The data are very similar to those characterizing the sample used for only 1 day (Figure 8). The EXAFS parameters are also very similar, as summarized in Table II. The data show that about 80% of the iridium was in the form of the carbonyl clusters in this used catalyst sample.

Infrared Results Characterizing the Decarbonylation of $[Ir_6(CO)_{16}]$ in NaY Zeolite. The zeolite incorporating $[Ir_6(CO)_{16}]$ with edge-bridging ligands was treated in flowing H_2 at 1 atm and 100 °C for 30 min. The infrared spectrum was unchanged.

(27) Kirlin, P. S.; van Zon, F. B. M.; Koningsberger, D. C.; Gates, B. C. *J. Phys. Chem.* **1990**, *94*, 8439.
(28) van Zon, J. B. A. D.; Koningsberger, D. C.; van't Blik, H. F. J.; Sayers, D. E. *J. Chem. Phys.* **1985**, *82*, 5742.
(29) Koningsberger, D. C.; Prins, R. *X-ray Absorption: Principles, Applications, Techniques of EXAFS, SEXAFS, and XANES*; Wiley: New York, 1988; p 395.

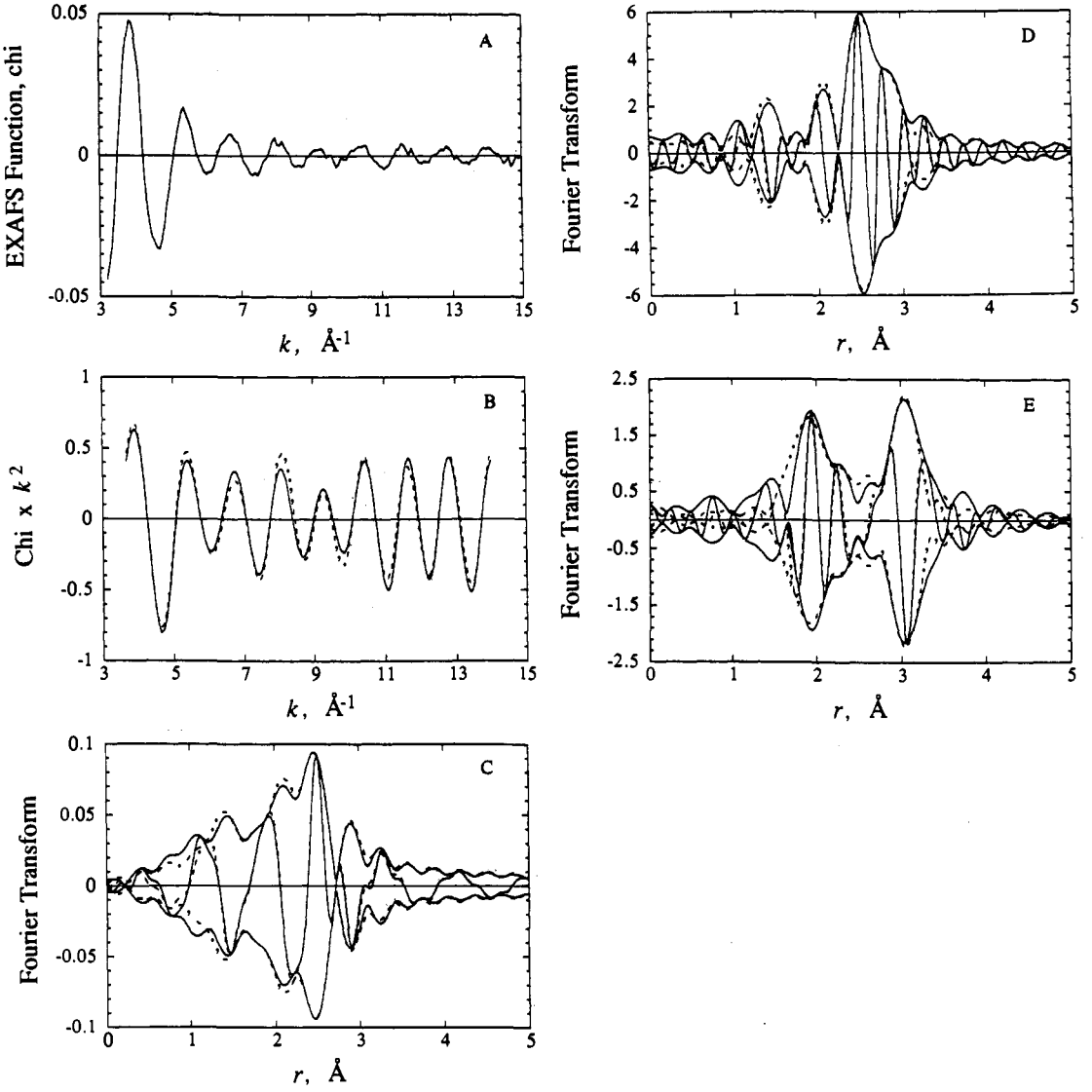

Figure 7. Results of EXAFS analysis obtained with the best calculated coordination parameters characterizing zeolite-supported Ir carbonyl after exposure to equimolar CO + H_2 at 20 atm and 250 °C for 1 day: (A) raw EXAFS data; (B) experimental EXAFS (solid line) and sum of the calculated Ir–Ir + Ir–C_t + Ir–C_b + Ir–O* + Ir–$O_{support}$ contributions (dashed line); (C) imaginary part and magnitude of Fourier transform (k^1 weighted, Δk = 3.80–13.80 Å^{-1}) of experimental EXAFS (solid line) and sum of the calculated Ir–Ir + Ir–C_t + Ir–C_b + Ir–O* + Ir–$O_{support}$ contributions (dashed line); (D) imaginary part and magnitude of Fourier transform (k^3 weighted, Δk = 3.80 – 13.80 Å^{-1}) of experimental EXAFS (solid line) and sum of the calculated Ir–Ir + Ir–C_t + Ir–C_b + Ir–O* + Ir–$O_{support}$ contributions (dashed line); (E) residual spectrum illustrating the contributions of carbonyl groups—imaginary part and magnitude of Fourier transform (k^3 weighted, Δk = 3.80–13.80 Å^{-1}) of raw data minus calculated Ir–Ir + Ir–$O_{support}$ EXAFS (solid line) and calculated Ir–C_t + Ir–C_b + Ir–O* EXAFS (dashed line).

Table I. EXAFS Results Characterizing the NaY Zeolite-Supported Iridium Carbonyl Species Prepared from [Ir(CO)$_2$(acac)] after Treatment in Equimolar CO + H_2 at 250 °C and 20 atm for 1 day[a,b]

shell	N	R, Å	$\Delta\sigma^2$, Å^2	ΔE_0, eV	EXAFS ref
Ir–Ir	3.50	2.77	0.0011	1.81	Pt–Pt
Ir–CO:					
Ir–C_t	1.98	1.89	0.0018	2.42	Ir–C
Ir–C_b	1.80	2.21	0.0010	−2.85	Ir–C
Ir–O*	1.82	3.02	0.0036	−5.05	Ir–O*
Ir–$O_{support}$	0.76	2.13	0.0030	−5.26	Pt–O

[a] Notation: N, coordination number for absorber–backscatterer pair; R, radial absorber–backscatterer distance; $\Delta\sigma^2$, Debye–Waller factor (difference with respect to reference compounds); ΔE_0, inner potential correction (correction of the edge position). [b] Estimated precision: N, ±20% (Ir–$O_{support}$, ±30%); R, ±2% (Ir–Ir, ±1%); $\Delta\sigma^2$, ±30%; ΔE_0, ±10%.

As the temperature increased beyond 125 °C, the bands broadened, decreased in intensity, and shifted to lower frequencies. After the sample had been held for 2 h at 300 °C in H_2, the carbonyl bands had disappeared, indicating that the sample had been decarbonylated. The decarbonylated sample was then evacuated at 300 °C for 30 min and cooled under vacuum to 25 °C; it was beige.

The zeolite incorporating [$Ir_6(CO)_{16}$] with face-bridging ligands was treated with H_2 in the same way. The sample was stable in H_2 at 100 °C for 30 min, but at higher temperatures the carbonyl bands decreased proportionately to each other in intensity, with only a slight change in frequencies. These bands disappeared after the sample had been held for 2 h in H_2 at 300 °C. The sample was then evacuated at 300 °C for 30 min and cooled under vacuum to room temperature; it was beige.

EXAFS Results Characterizing the Decarbonylated Iridium Clusters. The EXAFS data characterizing the decarbonylated sample formed from the isomer of [$Ir_6(CO)_{16}$] with face-bridging ligands (Figure 9A) were analyzed by a method that is nearly the same as that stated above for the used catalysts. The EXAFS data were Fourier transformed with k^2 weighting and no correction over the useful range (3.68 < k < 14.15 Å^{-1}). The major contributions were isolated by inverse Fourier transformation in the range 0.57 < r < 3.32 Å. The Ir–Ir contribution was estimated

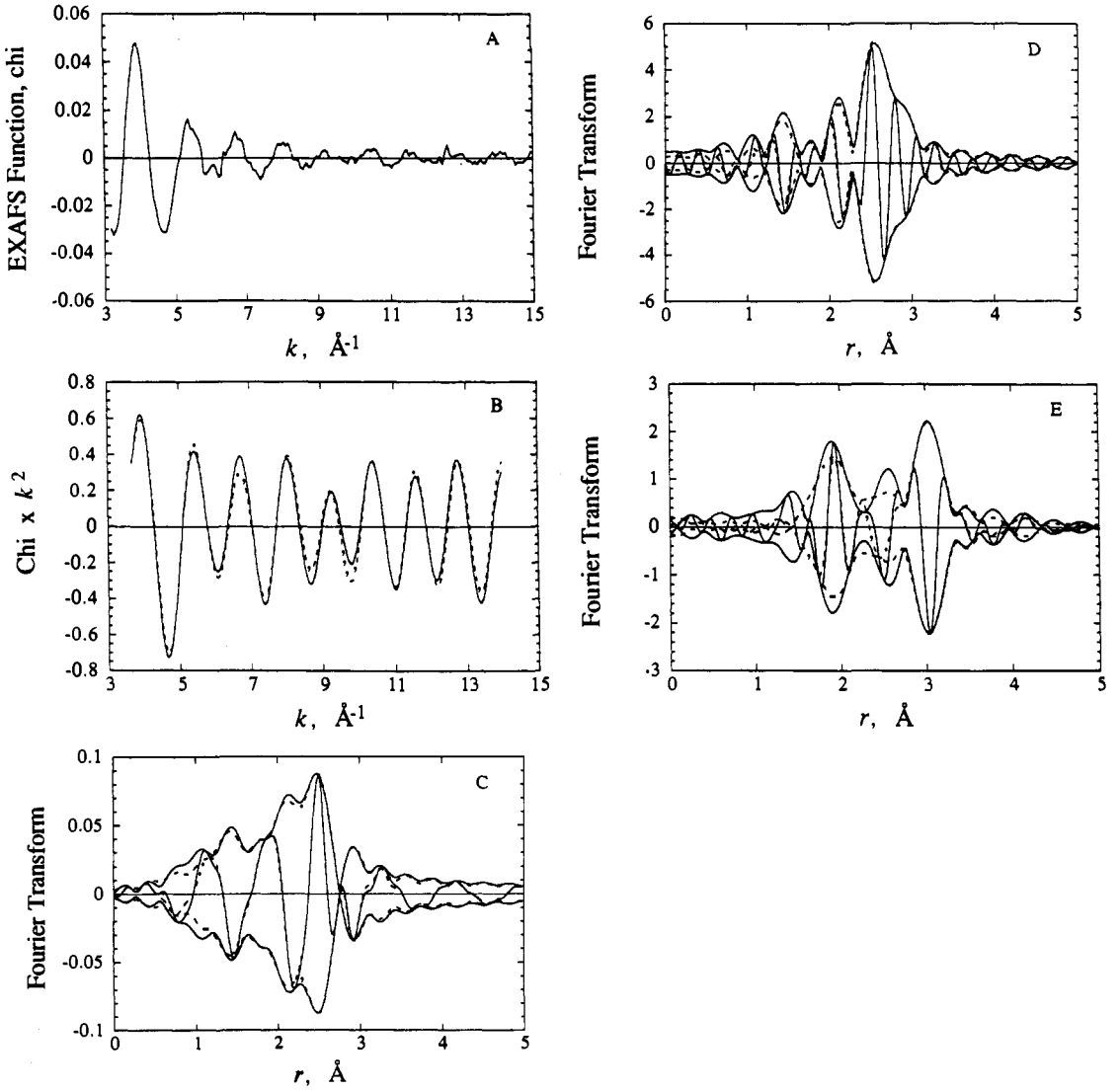

Figure 8. Results of EXAFS analysis obtained with the best calculated coordination parameters characterizing zeolite-supported Ir carbonyl after exposure to equimolar CO + H_2 at 20 atm and 250 °C for 8 days: (A) raw EXAFS data; (B) experimental EXAFS (solid line) and sum of the calculated Ir–Ir + Ir–C_t + Ir–C_b + Ir–O* + Ir–$O_{support}$ contributions (dashed line); (C) imaginary part and magnitude of Fourier transform (k^1 weighted, Δk = 3.80–13.80 Å^{-1}) of experimental EXAFS (solid line) and sum of the calculated Ir–Ir + Ir–C_t + Ir–C_b + Ir–O* + Ir–$O_{support}$ contributions (dashed line); (D) imaginary part and magnitude of Fourier transform (k^3 weighted, Δk = 3.80–13.80 Å^{-1}) of experimental EXAFS (solid line) and sum of the calculated Ir–Ir + Ir–C_t + Ir–C_b + Ir–O* + Ir–$O_{support}$ contributions (dashed line); (E) residual spectrum illustrating the contributions of carbonyl groups—imaginary part and magnitude of Fourier transform (k^3 weighted, Δk = 3.80–13.80 Å^{-1}) of raw data minus calculated Ir–Ir + Ir–$O_{support}$ EXAFS (solid line) and calculated Ir–C_t + Ir–C_b + Ir–O* EXAFS (dashed line).

Table II. EXAFS Results Characterizing the NaY Zeolite-Supported Iridium Carbonyl Species Formed after Treatment of the Sample Prepared from [$Ir(CO)_2$(acac)] in Equimolar CO + H_2 at 250 °C and 20 atm for 8 days[a,b]

shell	N	R, Å	$\Delta\sigma^2$, Å^2	ΔE_0, eV	EXAFS reference
Ir–Ir	3.24	2.77	0.0015	1.85	Pt–Pt
Ir–CO:					
Ir–C_t	1.71	1.89	0.0029	1.63	Ir–C
Ir–C_b	1.67	2.22	0.0017	−3.39	Ir–C
Ir–O*	1.78	3.01	0.0036	−5.86	Ir–O*
Ir–$O_{support}$	0.86	2.14	0.0038	−6.77	Pt–O

[a] Notation as in Table I. [b] Estimated precision: N, ±20% (Ir–$O_{support}$, ±30%); R, ±2% (Ir–Ir, ±1%); $\Delta\sigma^2$, ±30%; ΔE_0, ±10%.

by calculating an EXAFS function that agreed as closely as possible with the experimental results in the high-k range (7.5 < k < 14.0 Å^{-1}); the metal-support contributions in this region are small. An EXAFS function calculated with the first-guess parameters was then subtracted from the data, with the residual spectrum being expected to represent the Ir–$O_{support}$ interactions. The difference file was estimated with two Ir–O contributions, as both short[30,31] and long[32,33] metal–support oxygen distances have been frequently observed. As a first approximation, only four free parameters were estimated ($\Delta\sigma^2$, the Debye–Waller factor, and ΔE_0, the inner potential correction, were set equal to 0) to shorten the computational time.

The first-guess Ir–Ir and Ir–$O_{support}$ contributions were then added and compared with the raw data in r space, and the fit was not yet satisfactory. Then the Ir–$O_{support}$ contribution was subtracted from the data and better parameters for the Ir–Ir contribution were estimated. The improved fit for the Ir–Ir contribution was subtracted from the data, and more accurate parameters for the contributions of the metal–support interface were determined by fitting the metal–support contributions to

(30) Emrich, R. J.; Mansour, A. N.; Sayers, D. E.; McMillan, S. T.; Katzer, J. R. *J. Phys. Chem.* **1985**, *89*, 4261.
(31) Lytle, F. W.; Greegor, R. B.; Marques, E. C.; Via, G. H.; Sinfelt, J. H. *J. Catal.* **1985**, *95*, 546.
(32) Koningsberger, D. C.; van Zon, J. B. A. D.; van't Blik, H. F. J.; Visser, G. J.; Prins, R.; Mansour, A. N.; Sayers, D. E.; Short, D. R.; Katzer, J. R. *J. Phys. Chem.* **1985**, *89*, 4075.
(33) Koningsberger, D. C.; Martens, J. H. A.; Prins, R.; Short, D. R.; Sayers, D. E. *J. Phys. Chem.* **1986**, *90*, 3047.

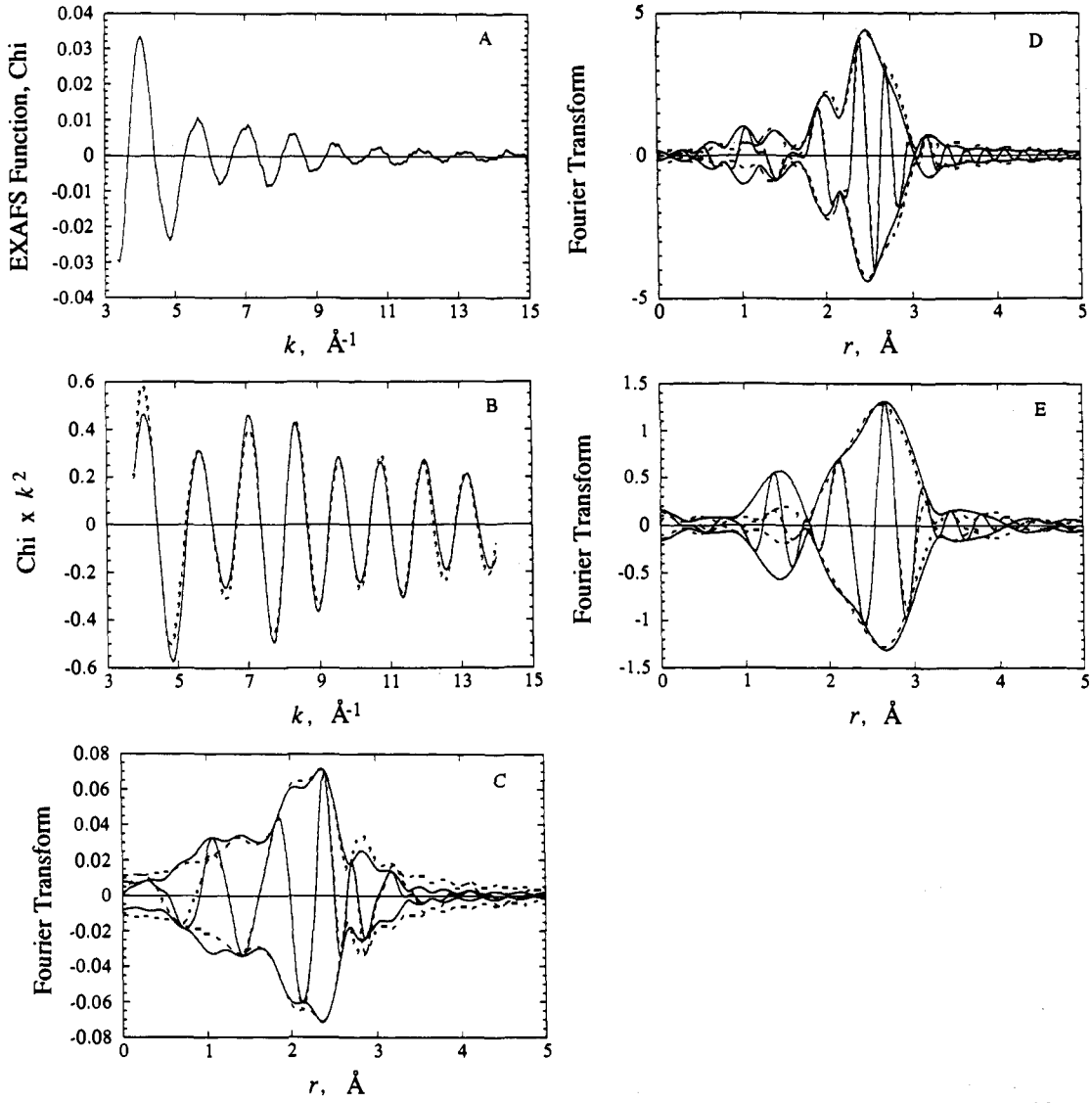

Figure 9. Results of EXAFS analysis obtained with the best calculated coordination parameters characterizing zeolite-supported Ir cluster prepared by decarbonylation of the Ir carbonyl cluster in NaY zeolite at 300 °C in H_2: (A) raw EXAFS data; (B) experimental EXAFS (solid line) and sum of the calculated Ir–Ir + Ir–C + Ir–$O_{support}$ contributions (dashed line); (C) imaginary part and magnitude of Fourier transform (k^1 weighted, Δk = 3.66–13.80 Å^{-1}) of experimental EXAFS (solid line) and sum of the calculated Ir–Ir + Ir–C + Ir–$O_{support}$ contributions (dashed line); (D) imaginary part and magnitude of Fourier transform (k^3 weighted, Δk = 3.66–13.80 Å^{-1}) of experimental EXAFS (solid line) and sum of the calculated Ir–Ir + Ir–C + Ir–$O_{support}$ contributions (dashed line); (E) residual spectrum illustrating the EXAFS contributions characterizing the metal–support interaction—imaginary part and magnitude of Fourier transform (k^3-weighted, Δk = 3.66–10.00 Å^{-1}) of raw data minus calculated Ir–Ir + Ir–C EXAFS (solid line) and calculated Ir–O_l + Ir–O_s EXAFS (dashed line).

the residual spectrum with all eight parameters; the initial guesses for parameter estimation were determined by adjusting the coordination parameters to give the best agreement with the residual spectrum, both in k space and in r space. Even after many iterations, the fit was not good in the low-r region. It was thus inferred that another small contribution, attributed to a low-Z backscatterer, had to be accounted for. A difference file was calculated by subtracting the best estimated Ir–Ir + Ir–$O_{support}$ contribution from the experimental EXAFS function. The additional contribution was calculated by fitting the difference file with four adjustable parameters. The additional low-Z scatterer is not identified; it may be carbon remaining from the carbonyl ligands, and we tentatively refer to the contribution as Ir–C.

The Ir–Ir, Ir–C, and two Ir–$O_{support}$ contributions were then added, representing the overall fit of the data. To show the goodness of the fit for both the high-Z (Ir) and low-Z (O, C) contributions, the raw data are compared with the fit in both k space (with k^2 weighting) and in r space (with both k^1 and k^3 weighting) (Figure 9B–D). The agreement is good.

Table III. EXAFS Results Characterizing the Iridium Clusters Formed by Decarbonylation of $[Ir_6(CO)_{16}]$ with Face-Bridging CO Ligands in NaY Zeolite at 300 °C in H_2[a,b]

shell	N	R, Å	$\Delta\sigma^2$, Å^2	ΔE_0, eV	EXAFS reference
Ir–Ir	3.60	2.71	0.0035	–2.00	Pt–Pt
Ir–$O_{support}$:					
Ir–O_s	1.01	2.17	0.0070	–6.20	Pt–O
Ir–O_l	1.85	2.71	0.0036	–6.11	Pt–O

[a] Notation as in Table I; the subscripts s and l refer to short and long, respectively. [b] Estimated precision: N, ±20% (Ir–O_l + Ir–O_s, ±30%); R, ±2% (Ir–Ir, ±1%); $\Delta\sigma^2$, ±30%; ΔE_0, ±10%.

The structure parameters are shown in Table III, and the Ir–$O_{support}$ contributions are shown in the difference file of Figure 9E. The number of parameters used to fit the data in this main-shell analysis is 16; the statistically justified number, calculated as above, is approximately 19.

Recarbonylation of the Decarbonylated Iridium Clusters. The decarbonylated sample formed from the $[Ir_6(CO)_{16}]$ isomer with face-bridging ligands (the used catalyst, Figure 10A) was exposed

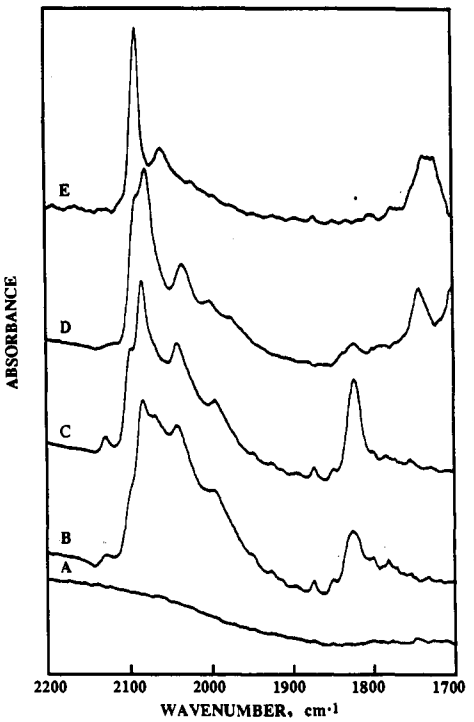

Figure 10. Infrared spectra characterizing the recarbonylation of the decarbonylated iridium cluster formed from treatment of $[Ir_6(CO)_{16}]$ with face-bridging ligands in NaY zeolite: (A) decarbonylated iridium cluster in NaY zeolite; (B) after treatment in CO at 125 °C for 2 h; (C) after treatment in CO at 125 °C for 6 h; (D) after treatment in CO at 175 °C for 2 h; and (E) after treatment in CO at 175 °C for 5 h.

to CO in the infrared cell as the temperature was raised. When the temperature reached 125 °C, infrared bands in the carbonyl region grew in at 2082, 2040, and 1815 cm^{-1} (Figure 10B). The growth in intensity continued for about 6 h, with the spectrum finally becoming virtually the same as that of the $[Ir_6(CO)_{16}]$ isomer with edge-bridging ligands (Figure 10C). Again, the sample was light yellow. When the sample was recarbonylated at temperatures >175 °C, a terminal band at 2098 cm^{-1} and a bridging carbonyl band at 1730 cm^{-1} appeared in the infrared spectrum, which is attributed to the $[Ir_6(CO)_{16}]$ cluster with face-bridging ligands (Figure 10D). After about 5 h at 175 °C, the spectrum became virtually the same as that of the $[Ir_6(CO)_{16}]$ cluster with face-bridging ligands (Figure 10E). These spectra show that the carbonylation–decarbonylation process was reversible; it was repeated three times with no noticable change in the infrared spectra of the carbonylated forms.

When the decarbonylated cluster formed from the isomer of $[Ir_6(CO)_{16}]$ with edge-bridging ligands was recarbonylated, the results were the same as those stated in the preceding two paragraphs.

EXAFS Results Characterizing Recarbonylated Iridium Carbonyl Clusters. The sample that had been formed by decarbonylation and subsequent recarbonylation of the zeolite incorporating the $[Ir_6(CO)_{16}]$ with face-bridging ligands was also characterized by EXAFS spectroscopy. The data are nearly the same as those characterizing the sample incorporating the original cluster with face-bridging ligands. The method of data analysis is virtually the same also. The results are shown in Figure 11 and summarized in Table IV. The results are almost identical to those presented for the sample prior to decarbonylation. These results confirm the conclusion from infrared spectroscopy that the decarbonylation-recarbonylation process was reversible.

Discussion

Evidence of $[Ir_6(CO)_{16}]$ in Zeolite Supercages: Parallels between Iridium Carbonyl Chemistry in Solution and in Zeolite Cages. $[Ir_4(CO)_{12}]$ is synthesized in solution by carbonylation of aqueous iridium salts[34-36] or by carbonylation of $[Ir(CO)_2(acac)]$ in undried THF.[37] Thus we suggest that water played a role in the synthesis of $[Ir_4(CO)_{12}]$. In basic solutions, the reductive carbonylation of $[Ir_4(CO)_{12}]$ with KOH in methanol under CO yields a family of iridium carbonyl cluster anions with nuclearities of 4, 6, and 8;[25] these clusters incorporate both terminal and bridging CO ligands. The reaction initially gives $[HIr_4(CO)_{11}]^-$ [38] and then $[Ir_8(CO)_{22}]^{2-}$ [39] and $[Ir_6(CO)_{15}]^{2-}$.[40,41] The latter is the most stable of these anionic species formed in the carbonylation of iridium precursors in basic solutions.[25,41] In acidic media, $[Ir_6(CO)_{15}]^{2-}$ is converted to $[Ir_6(CO)_{16}]$; both isomers mentioned above have been synthesized in this way.[22,25,41]

The basic surface of MgO is also an efficient medium for the synthesis of anionic metal carbonyl clusters.[42-45] This surface has also been used as a medium for synthesis, in the absence of solvents, of $[Os_5C(CO)_{14}]^{2-}$,[46] $[Os_{10}C(CO)_{24}]^{2-}$,[46,47] $[HIr_4(CO)_{11}]^-$,[42,45] $[Ir_8(CO)_{22}]^{2-}$,[44,45] and $[Ir_6(CO)_{15}]^{2-}$;[43,45] the anions could be extracted from the surface by cation metathesis. The chemistry of osmium and iridium carbonyl clusters on the surface of MgO closely parallels the chemistry of these metal carbonyl clusters in basic solutions. Some of these anionic carbonyl clusters have been shown to be stabilized on the MgO surface during catalytic CO hydrogenation.[47,48]

Similarly, it has also been shown that the supercages of NaX zeolites are sufficiently basic to provide an efficient medium for the synthesis of anionic iridium carbonyl clusters.[6] These cages have been used as a medium for synthesis of $[HIr_4(CO)_{11}]^-$ and $[Ir_6(CO)_{15}]^{2-}$ in good yields. The chemistry of iridium carbonyl clusters in the cages of NaX zeolite parallels the chemistry of the metal carbonyl clusters in basic solutions and on the basic MgO support. The $[Ir_6(CO)_{15}]^{2-}$ cluster in NaX zeolite has also been shown to be maintained during catalytic CO hydrogenation.[6,16]

On the weakly basic γ-Al_2O_3 surface, however, the chemistry of metal carbonyls is different, being similar to that occurring in nonbasic solutions. For example, iridium precursors react on the γ-Al_2O_3 surface in the presence of CO to give $[Ir_4(CO)_{12}]$.[37] The formation of neutral iridium carbonyl clusters reported here in the NaY zeolite is evidently similar to that occurring on the γ-Al_2O_3 surface. The result is not surprising because NaY zeolite is less basic than NaX zeolite (the Si/Al atomic ratio of the NaX was about 2.5 and that of the NaY was about 5.0). These results give an indication of the possibilities for modification of the reactivity in the solvent-like cages of the zeolites by changing the Si to Al ratio.

Since $[Ir_4(CO)_{12}]$ and the two isomers of $[Ir_6(CO)_{16}]$ are slightly soluble in THF, the lack of extraction of these clusters from NaY zeolite with THF indicates that the clusters were trapped in the zeolite cages. The results are consistent with a

(34) Malatesta, L.; Caglio, G.; Angoletta, M. *Inorg. Synth.* **1972**, *13*, 95.
(35) Della Pergola, R.; Garlaschelli, L.; Martinengo, S. *J. Organomet. Chem.* **1987**, *331*, 271.
(36) Pruchnik, F. P.; Wajda-Hermanowicz, K.; Koralewicz, M. *J. Organomet. Chem.* **1990**, *384*, 381.
(37) Kawi, S.; Chang, J.-R.; Gates, B. C. *J. Phys. Chem.*, in press.
(38) Bau, R.; Chiang, M. Y.; Wei, K.; Garlaschelli, K.; Martinengo, S.; Koetzle, T. F. *Inorg. Chem.* **1984**, *23*, 4758.
(39) Demartin, F.; Manassero, M.; Garlaschelli, L.; Raimondi, C.; Martinengo, S.; Canziani, F. *J. Chem. Soc., Chem. Commun.* **1981**, 528.
(40) Demartin, F.; Manassero, M.; Sansoni, M.; Garlaschelli, L.; Martinengo, S. *J. Chem. Soc., Chem. Commun.* **1980**, 903.
(41) Stevens, R. E.; Lin, P. C. C.; Gladfelter, W. L. *J. Organomet. Chem.* **1985**, *287*, 133.
(42) Maloney, S. D.; van Zon, F. B. M.; Koningsberger, D. C.; Gates, B. C. *Catal. Lett.* **1990**, *5*, 161.
(43) Maloney, S. D.; Kelley, M. J.; Koningsberger, D. C.; Gates, B. C. *J. Phys. Chem.* **1991**, *95*, 9406.
(44) Maloney, S. D.; Kelley, M. J.; Gates, B. C. *J. Organomet. Chem.* **1992**, *435*, 377.
(45) Kawi, S.; Gates, B. C. *Inorg. Chem.* **1992**, *31*, 2939.
(46) Lamb, H. H.; Fung, A. S.; Tooley, P. A.; Puga, J.; Krause, T. R.; Kelley, M. J.; Gates, B. C. *J. Am. Chem. Soc.* **1989**, *111*, 8367.
(47) Lamb, H. H.; Gates, B. C. *J. Am. Chem. Soc.* **1986**, *108*, 81.
(48) Kawi, S.; Gates, B. C., to be published.

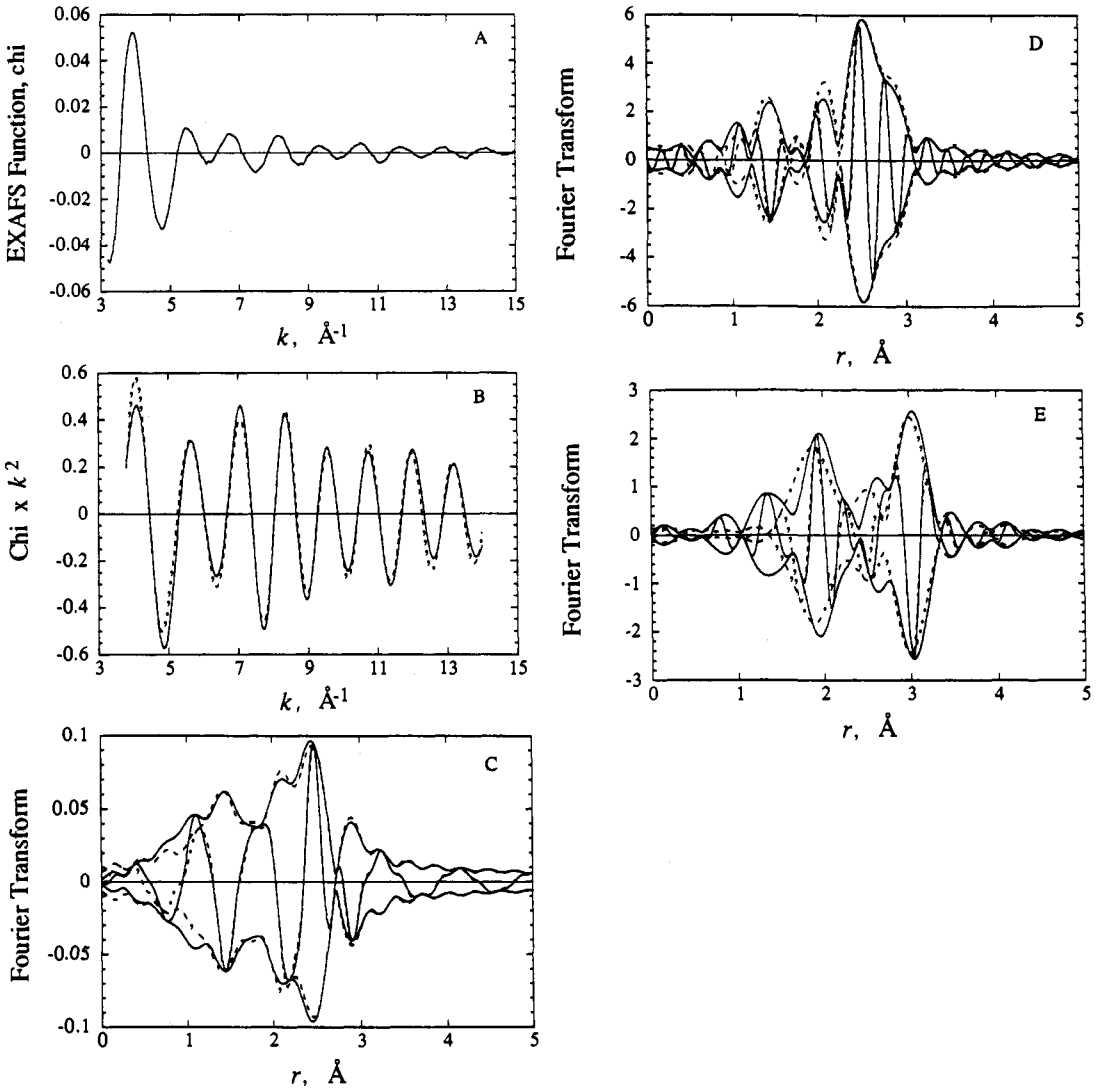

Figure 11. Results of EXAFS analysis obtained with the best calculated coordination parameters characterizing the recarbonylation of the decarbonylated iridium cluster formed from treatment of $[Ir_6(CO)_{16}]$ with face-bridging ligands in NaY zeolite: (A) raw EXAFS data; (B) experimental EXAFS (solid line) and sum of the calculated Ir–Ir + Ir–C_t + Ir–C_b + Ir–O* + Ir–$O_{support}$ contributions (dashed line); (C) imaginary part and magnitude of Fourier transform (k^1 weighted, Δk = 3.80–13.80 Å^{-1}) of experimental EXAFS (solid line) and sum of the calculated Ir–Ir + Ir–C_t + Ir–C_b + Ir–O* + Ir–$O_{support}$ contributions (dashed line); (D) imaginary part and magnitude of Fourier transform (k^3 weighted, Δk = 3.80–13.80 Å^{-1}) of experimental EXAFS (solid line) and sum of the calculated Ir–Ir + Ir–C_t + Ir–C_b + Ir–O* + Ir–$O_{support}$ contributions (dashed line); (E) residual spectrum illustrating the contributions of carbonyl groups—imaginary part and magnitude of Fourier transform (k^3 weighted, Δk = 3.80–13.80 Å^{-1}) of raw data minus calculated Ir–Ir + Ir–$O_{support}$ EXAFS (solid line) and calculated Ir–C_t + Ir–C_b + Ir–O* EXAFS (dashed line).

Table IV. EXAFS Results Characterizing the Species Formed by CO Treatment of Decarbonylated Iridium Clusters in NaY Zeolite[a,b]

shell	N	R, Å	$\Delta\sigma^2$, Å^2	ΔE_0, eV	EXAFS reference
Ir–Ir	3.40	2.76	0.0013	–0.80	Pt–Pt
Ir–CO:					
Ir–C_t	1.99	1.85	0.0023	4.70	Ir–C
Ir–C_b	1.60	2.24	0.0022	–5.46	Ir–C
Ir–O*	1.69	2.99	0.0027	–5.80	Ir–O*
Ir–$O_{support}$[c]	0.82	2.10	0.0045	–8.00	Pt–O

[a] Notation as in Table I. [b] Estimated precision: N, ±20% (Ir–$O_{support}$, ±30%); R, ±2% (Ir–Ir, ±1%); $\Delta\sigma^2$, ±30%; ΔE_0, ±10%. [c]

ship-in-a-bottle synthesis in the zeolite supercages. The precursor $[Ir(CO)_2(acac)]$ is small enough to fit through the zeolite apertures and diffuse into the interior of the zeolite crystallites. Even larger metal carbonyls have been shown to fit: $[CpM(CO)_2]$, $[Cp^*M(CO)_2]$, and $[CpM(C_2H_4)_2]$ [M = Rh, Ir, Cp = C_5H_5; Cp* = $(CH_3)_5C_5$].[49] $[Ir_4(CO)_{12}]$ (with a diameter of about 9 Å) and the two isomers of $[Ir_6(CO)_{16}]$ (with diameters of about 11 Å) are small enough to fit in the supercages of zeolite Y (which have diameters of about 12 Å) but too large to fit in the sodalite cages and too large to diffuse rapidly through the apertures (which have diameters of about 7.4 Å). Thus it is concluded that the clusters were trapped in the supercages and not removed when the sample came in contact with THF.

Confirmation of Structure of Zeolite-Entrapped $[Ir_6(CO)_{16}]$ by EXAFS Spectroscopy. Both the infrared and EXAFS results are consistent with the inference that the iridium carbonyl species formed in high yield from $[Ir(CO)_2(acac)]$ in NaY zeolite after treatment in equimolar CO + H_2 at 20 atm and 250 °C for 1 day was the isomer of $[Ir_6(CO)_{16}]$ with face-bridging CO ligands. The evidence for this cluster is the following: (1) the close agreement between the infrared spectrum of the zeolite-supported iridium carbonyl and that of the THF solution of the isomer of $[Ir_6(CO)_{16}]$ with face-bridging CO ligands (however, infrared spectra are usually not sufficient to identify metal carbonyls in zeolites[21]) and (2) the EXAFS spectrum of the zeolite-entrapped iridium carbonyl.

The EXAFS results provide the strongest evidence, showing that the backscatterers in the immediate vicinity of the Ir absorber

(49) Ozin, G. A.; Haddleton, D. M.; Gil, C. J. *J. Phys. Chem.* **1989**, *93*, 6710.

atoms in the zeolite-supported iridium carbonyl included Ir and low-Z backscatterers identified by the multiple scattering effect as C and O*. We infer, as follows, that the relative contributions of these backscattering atoms support the identification of the zeolite-entrapped species as $[Ir_6(CO)_{16}]$: All the Ir atoms in crystalline $[Ir_6(CO)_{16}]$ with face-bridging ligands are stereochemically equivalent, with each bonded to four Ir atoms at an average distance of 2.779 Å, to two terminal carbonyl ligands with an average Ir–C_t distance of 1.886 Å, and to two bridging carbonyl ligands with an average Ir–C_b distance of 2.20 Å.[22] The EXAFS results characterizing the supported iridium carbonyl (Table I) match, within experimental error, the crystallographic data for $[Ir_6(CO)_{16}]$ with face-bridging ligands. They indicate an Ir–Ir coordination number of 3.5 (which is equal to 4, within the experimental error of 20%) with an average Ir–Ir distance of 2.77 Å, an Ir–C_t coordination number of 2.0 with an average distance of 1.89 Å, and an Ir–C_b coordination number of 1.8 with an average distance of 2.21 Å.

Although the structural data characterizing the Ir–Ir, Ir–C_t, and Ir–C_b interactions agree well with the crystallographic data, the results characterizing the Ir–O* interaction (Table I) do not. The discrepancy between the sum of the Ir–C_t (2.0) and Ir–C_b (1.8) coordination numbers, on the one hand, and the Ir–O* coordination number (1.8), on the other, can be understood on the basis of multiple scattering effects,[43,50] as follows: The positions of the oxygens of the terminal and bridging carbonyl ligands in the crystalline $[Ir_6(CO)_{16}]$ with face-bridging ligands are known.[22] The crystallographic distance between the Ir and O atoms of the terminal carbonyl ligands is virtually the same as the crystallographic distance between the Ir and O atoms of bridging carbonyl ligands. However, the Ir–C–O_t angle is 177°, whereas the Ir–C–O_b angle is 133°.[22] When the Ir–C–O bond angle is greater than approximately 140°, the EXAFS phase shift and amplitude function depend strongly on the positions of the atoms because of multiple scattering effects.[50] In contrast, the multiple scattering effect is not expected to be significant for bridging carbonyl oxygens in $[Ir_6(CO)_{16}]$, since the Ir–C–O_b angle is only 133°. Since the terminal and bridging carbonyl oxygen atoms are located at nearly the same distance from Ir, it is difficult to separate the two contributions in the EXAFS analysis and to determine an accurate estimate of the overall Ir–O* coordination number. Consequently, we infer that the discrepancy between the sum of the Ir–C_t and Ir–C_b coordination numbers and the Ir–O* coordination numbers determined by the EXAFS data is a result of there being two types of carbonyl oxygen contributions at nearly the same distance but experiencing different degrees of multiple scattering that lead to different phase shifts, which may give a negative interference and a low estimate of the Ir–O* coordination number.

Thus the EXAFS data are consistent with the infrared data and the conclusion that $[Ir_6(CO)_{16}]$ with face-bridging ligands was present in the zeolite. The EXAFS data are not consistent with the presence of significant amounts of the isomer of $[Ir_6(CO)_{16}]$ with edge-bridging CO ligands, which would be characterized by an Ir–C_b coordination number of 1.33 in contrast to the observed value of 1.8.

There was another contribution evident in the EXAFS data, indicating the presence of a small amount of an Ir-containing species in addition to $[Ir_6(CO)_{16}]$. The additional contribution was needed for a good fit of the EXAFS data. It may arise from unconverted $[Ir(CO)_2(acac)]$ or other mononuclear species.[22,51-53] The results indicate that more than 85% of the Ir atoms were present in the $[Ir_6(CO)_{16}]$ clusters.

Scheme I. Chemistry of Iridium Clusters in NaY Zeolite[a]

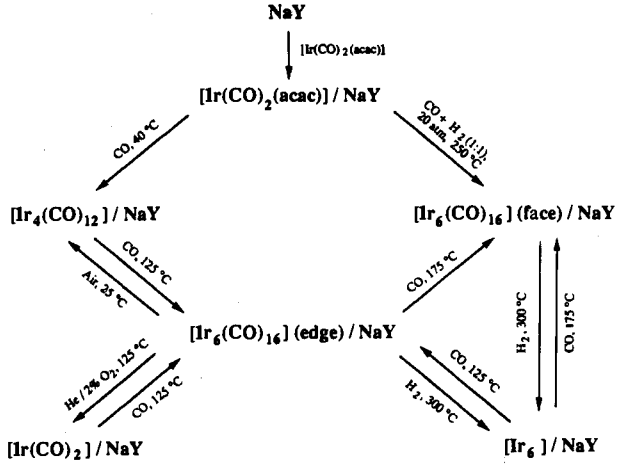

[a] The terms edge and face refer to the isomers with edge- and face-bridging carbonyl ligands, respectively.

In summary, there is good agreement between the EXAFS results characterizing the sample formed from $[Ir(CO)_2(acac)]$ in NaY zeolite after treatment in CO + H_2 at 250 °C and 20 atm for 1 day (Table I) and the crystal structure of the isomer of $[Ir_6(CO)_{16}]$ with face-bridging ligands.[22] We conclude, therefore, that the predominant entrapped species in NaY zeolite after treatment in high-pressure CO + H_2 was $[Ir_6(CO)_{16}]$ with face-bridging CO ligands. The intrazeolite chemistry is summarized in Scheme I.

Others[54] have also reported the formation of $[Ir_6(CO)_{16}]$ in NaY zeolite from a mononuclear iridium carbonyl in the presence of CO. However, the conclusions were based only on infrared spectra, and the authors did not distinguish which isomers of the cluster were present.

Interactions of Iridium Carbonyl Clusters with the NaY Zeolite Framework. The isomer of $[Ir_6(CO)_{16}]$ with face-bridging CO ligands in NaY zeolite is characterized by principal ν_{CO} bands at 2098 s, 2066 w, and 1730 cm^{-1}. The 2098- and 2066-cm^{-1} bands are assigned to the symmetric and asymmetric stretching of the two CO ligands bound to each Ir atom in $[Ir_6(CO)_{16}]$. The 1730-cm^{-1} band corresponds to the four face-bridging CO ligands, each bound to three Ir atoms. The stretching frequency of the terminal CO ligand is shifted to higher energy by about 20 cm^{-1} and that of the face-bridging CO ligand is shifted to lower energy by about 35 cm^{-1} than those of the same isomer of $[Ir_6(CO)_{16}]$ in THF solution.

Similar trends in the infrared band shifts have been observed for the isomer of $[Ir_6(CO)_{16}]$ that has edge-bridging CO ligands in NaY zeolite, which is characterized by principal carbonyl infrared bands at 2082 s, 2040 m, and 1816 m cm^{-1}. The 2082- and 2040-cm^{-1} bands are assigned to the symmetric and asymmetric stretching of the two terminal CO ligands bound to each Ir atom in $[Ir_6(CO)_{16}]$. The 1816-cm^{-1} band corresponds to the four edge-bridging CO ligands, each bound to two Ir atoms. The stretching frequency of the terminal CO bond is shifted to higher energy by approximately 5 cm^{-1} and that of the edge-bridging CO ligand is shifted to lower energy by approximately 10 cm^{-1} than those of the same isomer $[Ir_6(CO)_{16}]$ in THF solution.

These shifts of the terminal and bridging carbonyl bands observed with both isomers of $[Ir_6(CO)_{16}]$ in NaY zeolite are similar to the shifts observed for metal carbonyls in solutions containing Lewis acids such as $Al(C_2H_5)_3$, which have been examined extensively.[55,56] A general pattern appears to be the following: Interaction of a metal carbonyl with a Lewis acid via

(50) van Zon, F. B. M.; Kirlin, P. S.; Gates, B. C.; Koningsberger, D. C. *J. Phys. Chem.* **1989**, *93*, 2218.
(51) Rao, L.-F.; Fukuoka, A.; Kosugi, N.; Kuroda, H.; Ichikawa, M. *J. Phys. Chem.* **1990**, *94*, 5317.
(52) Yates, J. T., Jr.; Duncan, T. M.; Vaughan, R. M. *J. Chem. Phys.* **1979**, *71*, 3908.
(53) Wang, H. P.; Yates, J. T., Jr. *J. Catal.* **1984**, *89*, 79.
(54) Gelin, P.; Lefebvre, F.; Elleuch, B.; Naccache, C.; Ben Taarit, Y. *ACS Symp. Ser.* **1985**, *218*, 469.
(55) Shriver, D. F. *J. Organomet. Chem.* **1975**, *94*, 259.
(56) Horwitz, C. P.; Shriver, D. F. *Adv. Organomet. Chem.* **1984**, *23*, 219.

the oxygen of a carbonyl group typically results in a large decrease of the infrared absorption frequency of the carbonyl group, with the stretching frequencies of the noninteracting carbonyl ligands all shifting to slightly higher frequencies. For example, Shriver and co-workers[55,56] reported shifts of terminal and bridging carbonyl bands resulting from adduct formation between compounds such as $[(C_5H_5)Fe(CO)_2]_2$ and Lewis acids such as $Al(C_2H_5)_3$, which led to shifts of 100–300 cm^{-1} to lower energy of the bridging carbonyl bands and shifts of 30–70 cm^{-1} to higher energy of the terminal carbonyl bands. Similar shifts have been observed for $[Rh_6(CO)_{16}]$ in NaY zeolite and attributed to the interactions of the oxygen atoms of the face-bridging carbonyl ligands with the Lewis acid sites (Al^{3+} ions).[51]

The basicity of the oxygen in carbonyl ligands of metal clusters depends on the CO coordination geometry;[57] triply bridging carbonyl ligands are more basic than doubly bridging carbonyl ligands, which are significantly more basic than terminal carbonyl ligands. This pattern is borne out in the present results; the relatively large shifts in the stretching frequency of the face-bridging ligands in $[Ir_6(CO)_{16}]$ compared with the edge-bridging carbonyl ligands in this cluster in NaY zeolite indicate a stronger interaction of Lewis acid sites with the oxygen of face-bridging CO ligands than with the oxygen of edge-bridging CO ligands. Such an interaction is expected to result in a net withdrawal of electrons from the cluster, decreasing the back bonding to the terminal carbonyl ligands, strengthening the C–O bonds, and shifting the ν_{CO} bands of the terminal carbonyl ligands to higher frequencies. $[Ir_4(CO)_{12}]$ in the zeolite, which has only terminal carbonyl ligands, is not characterized by significant shifts in the C–O stretching frequencies, consistent with the weak basicity of the ligands (Figure 1B).

In summary, the interactions of the carbonyl ligands of iridium carbonyl clusters with the Lewis acid sites in zeolites are indicated by shifts in the stretching frequencies of the CO ligands, and the pattern parallels that observed for metal carbonyl clusters in solutions containing Lewis acids.

Reactivity of Iridium Carbonyl Clusters in NaY Zeolite Cages. When the zeolite-supported $[Ir_6(CO)_{16}]$ with edge-bridging ligands was treated with oxygen, a reaction occurred to produce a species characterized by two sharp carbonyl bands, at 2083 and 2000 cm^{-1}. The new iridium carbonyl species is assigned as an $Ir^I(CO)_2$ complex on the basis of the comparison of its infrared spectrum with, for example, the spectrum of $[Ir(CO)_2(acac)]$ and that of $[Rh(CO)_2Cl]_2$.[58] We infer that there was an oxidative fragmentation of iridium carbonyl clusters to form iridium subcarbonyls in the zeolite. Such reactions on the surfaces of amorphous metal oxides have been investigated extensively and used to synthesize nearly uniform, isolated surface-bound ensembles having the nuclearity of the cluster precursor.[57,59,60] There is a parallel between the oxidative fragmentation of supported metal carbonyl clusters and the disruption of small supported aggregates of metal resulting from exposure to CO.[57]

The oxidized Ir carbonyl species in NaY zeolite could be reductively carbonylated by treatment in CO to give the isomer of $[Ir_6(CO)_{16}]$ with edge-bridging ligands, and the cycle could be repeated many times. The repeatability of the oxidative-fragmentation/reductive-carbonylation cycle suggests that the environment of the zeolite cages played a role in preventing the mononuclear iridium carbonyl species from migrating out of the zeolite pores to the outer zeolite surface, thereby hindering the formation of larger iridium clusters and even crystallites.

Metal carbonyl compounds are well-known examples of fluxional molecules,[61] and some adopt different isomer forms in solution. The data characterizing the reductive carbonylation of iridium carbonyls in the zeolite cages show that the isomer of $[Ir_6(CO)_{16}]$ with edge-bridging ligands was formed at a lower temperature than the isomer of $[Ir_6(CO)_{16}]$ with face-bridging ligands. The observation suggests that the edge-bridging species may be an intermediate in the conversion of the mononuclear iridium carbonyl to the isomer of $[Ir_6(CO)_{16}]$ with face-bridging carbonyl groups.

Although isomers of $[Ir_6(CO)_{16}]$,[22] $[Co_2(CO)_8]$,[62] and $[H_3Ru_4(CO)_{12}]^-$ [63] have been crystallographically characterized, the present work represents the first evidence of two different isomers of a metal carbonyl cluster in a cage. The conversion of one of the isomers of $[Ir_6(CO)_{16}]$ to the other (and the interconversion of $[Ir_6(CO)_{16}]$ and $[Ir_4(CO)_{12}]$) in NaY zeolite cages suggests that the zeolite cages have a solvent-like character. They may be advantageous media for synthesis of new structures: When the isomers of $[Ir_6(CO)_{16}]$ were synthesized in solution, only 10% yields of each were observed;[22,25] a 60% yield was obtained with a tedious method.[41] In contrast, the isomer of this cluster with face-bridging ligands was synthesized in approximately 85% yield in the zeolite cages. Zeolite cages appear to facilitate the synthesis of palladium carbonyl clusters that are not known in the soluble or crystalline states.[5,64] However, there is no known way to remove the clusters intact from the cages.

Evidence That Iridium Carbonyls Were Trapped in Zeolite Cages and Not Present Outside Zeolite Crystallites. One of the main issues complicating the synthesis and characterization of metal clusters in zeolites is the simultaneous formation of metal clusters or crystallites outside the zeolite crystallites, which is apparently often unavoidable. Much of the reported work with metal clusters and other nanostructures in zeolites has failed to include evidence to establish whether all the clusters were actually confined in the cages.

The results of the work summarized here are consistent with the inference that virtually all the iridium clusters were formed in and confined to the zeolite cages. The evidence is as follows:

(1) The synthesis conditions were chosen to remove iridium precursors and clusters from the outside of the zeolite crystals. The use of the neutral precursor $[Ir(CO)_2(acac)]$ has the advantage of allowing removal of unconverted precursor that remained outside the crystallites by thorough washing with hexane; the infrared spectra indicate that the washing did not remove all the $[Ir(CO)_2(acac)]$ from the sample. Hence, we infer that the precursor remaining after the washing was inside the zeolite cages. Thus we infer that these precursors were the source of the iridium carbonyl clusters, which were entrapped in the zeolite cages.

(2) The lack of success in extraction of the iridium carbonyl clusters from the samples is consistent with the entrapment of the clusters, consistent with the fact that the clusters are too large to fit through the zeolite apertures. In contrast, iridium carbonyl clusters could be extracted readily from surfaces of metal oxide supports (MgO[45] and γ-Al_2O_3[37]) that have pores large enough to allow the rapid diffusion of the clusters.

(3) The evidence of interactions of both isomers of $[Ir_6(CO)_{16}]$ with cations of the support (evidence from the infrared spectra) is consistent with interactions of the CO ligands with Na^+ ions, which are exchangeable ions located in the zeolite cages.

(4) The reversibility of the cycles of oxidative fragmentation and reductive carbonylation of the iridium carbonyls might not be expected to occur if the iridium species were not in uniform environments such as those provided by the zeolite cages, which we infer help to stabilize the fragmented species and prevent their agglomeration to form particles of iridium metal. In contrast,

(57) Lamb, H. H.; Gates, B. C.; Knözinger, H. *Angew. Chem., Int. Ed. Engl.* **1988**, *27*, 1127.
(58) Smith, A. K.; Hugues, F.; Theolier, A.; Basset, J. M.; Ugo, R.; Zanderighi, G. M.; Bilhou, J. L.; Bilhou-Bougnol, V.; Graydon, W. F. *Inorg. Chem.* **1979**, *18*, 3104.
(59) Gates, B. C. In *Catalyst Design: Progress and Perspectives*; Hegedus, L. L., Ed.; Wiley: New York, 1987; p 71.
(60) Gates, B. C.; Lamb, H. H. *J. Mol. Catal.* **1989**, *52*, 1.
(61) Cotton, F. A. *J. Organomet. Chem.* **1975**, *100*, 29.
(62) Lichtenberger, D. L.; Brown, T. L. *Inorg. Chem.* **1978**, *17*, 1381.
(63) Jackson, P. F.; Johnson, B. F. G.; Lewis, J.; McPartlin, M.; Nelson, W. J. H. *J. Chem. Soc., Chem. Commun.* **1978**, 920.
(64) Zhang, Z.; Sachtler, W. M. H. *J. Mol. Catal.* **1991**, *67*, 349.

$[Ir_4(CO)_{12}]$ formed on γ-Al_2O_3[37,65] and SiO_2,[65,66] for example, could not be reversibly fragmented and reformed; instead, Ir particles formed.

Catalytic Hydrogenation of CO. The NaY zeolite-supported Ir catalyst is characterized by an unusual selectivity in CO hydrogenation; it gave a non-Schulz–Flory distribution of hydrocarbon products (with high yields of propane), which contrasts with the Schulz–Flory distribution that is characteristic of alumina-supported iridium crystallites and virtually all conventional supported metal catalysts. Similar non-Schulz–Flory distributions have been observed with NaY zeolite-supported osmium carbonyl[13,14] and rhodium carbonyl[15] catalysts as well as NaX zeolite-supported iridium carbonyl catalysts.[16] The predominant form of the metal in each of these zeolite-supported catalysts was suggested to be a metal carbonyl cluster. These results are consistent with the suggestion that the catalytically active species were metal carbonyl clusters entrapped in the zeolite cages, which are evidently catalytically distinct from conventional supported metals.

However, the results do not exclude the possibility of catalysis by undetected small Ir crystallites present with the iridium carbonyl clusters in the catalyst. Since the activity of the catalyst is low and the activity of Ir metal is relatively high, the observed activity could be explained by only a small amount of Ir metal.

The stability of the zeolite-supported catalysts may be attributed to the stabilization of the metal clusters associated with (1) the strength of the metal–metal bonds, (2) the CO ligands provided by the gas-phase reactant, and (3) the geometry of the zeolite pores, with relatively large cages (diameter = 12 Å) and small apertures (diameter = 7.4 Å) which entrap the clusters and hinder their sintering into unselective metal particles.[13,14]

Pressure was found to be crucial for stable performance of these zeolite-supported catalysts. The results characterizing the iridium-containing catalyst reported here show that a pressure of 20 atm of equimolar CO + H_2 was sufficient to maintain the catalytic performance for at least 1 day. The contrasting results obtained at low pressure indicate that the high pressure of CO is needed to maintain the carbonyl clusters during catalytic CO hydrogenation and thus maintain the catalytic performance. The infrared results obtained at 1 atm of CO + H_2 show that the hexairidium carbonyl clusters could not be maintained at temperatures >240 °C; they agglomerated to form metal particles.

The catalyst that had been used with a feed containing a 1/3 molar CO:H_2 ratio at 20 atm was black at the upstream end of the catalyst bed, suggesting that Ir metal particles had formed on the zeolite outer surface. We infer that under the relatively high H_2 partial pressure and low CO partial pressure, the zeolite-supported iridium carbonyl species fragmented and migrated out through the apertures of the zeolite.[14] The product distribution data characterizing the catalytic reaction are typical of a conventional supported metal catalyst, giving the Schulz–Flory distribution of hydrocarbon products. These results are consistent with the inference that the catalytically active species in the more selective catalysts (those not exposed to low CO/H_2 ratios) were trapped in the zeolite cages.

Stability of $[Ir_6(CO)_{16}]$ during Catalytic CO Hydrogenation. As shown in preceding sections, it is apparent that the catalyst after being used in equimolar CO + H_2 at 20 atm for 1 day contained predominantly $[Ir_6(CO)_{16}]$ with face-bridging ligands. The infrared results characterizing the catalyst that had been used for 8 days were indistinguishable from those characterizing the catalyst used for only 1 day. The EXAFS results characterizing the two used catalysts (Tables I and II) indicate, within experimental error, the same amount of $[Ir_6(CO)_{16}]$; about 80% of the iridium was in the form of these clusters in the used catalysts.

The maintenance of the activity and selectivity of the catalyst and the lack of change in the amount of $[Ir_6(CO)_{16}]$ are consistent with the suggestion that the isomer of $[Ir_6(CO)_{16}]$ with face-bridging ligands might be the catalyst precursor; however, there are not sufficient data for identification of the catalytically active species.

Decarbonylation of $[Ir_6(CO)_{16}]$ Entrapped in NaY Zeolite. The decarbonylation of $[Ir_6(CO)_{16}]$ in NaY zeolite was carried out in flowing H_2 by gradually increasing the temperature. The terminal absorption bands in the infrared spectrum decreased in intensity, broadened, and shifted to lower frequency as the temperature increased. This result is similar to those of Handy et al.,[67] who observed that both the terminal and the bridging bands shifted to lower energy as the degree of decarbonylation of $[Pt_{15}(CO)_{30}]^{2-}$ (present as the PPN salt) on γ-Al_2O_3 increased with the sample in flowing He. The decrease of CO coverage leads to a diminished dipole–dipole coupling between adjacent CO molecules and a lower energy shift of the CO absorption bands.[68]

To investigate the structure of the clusters resulting from the decarbonylation, the sample was characterized by EXAFS spectroscopy. The Ir–Ir coordination number characteristic of the sample prepared by decarbonylation of $[Ir_6(CO)_{16}]$ in NaY zeolite (Table III), 3.6, is the same, within experimental error, as the crystallographically determined Ir–Ir coordination number of $[Ir_6(CO)_{16}]$ (4). The result suggests that the structure of the Ir cluster frame after decarbonylation resembles that of the octahedral frame of $[Ir_6(CO)_{16}]$. The lack of EXAFS evidence of the remaining (higher-shell) Ir atom in the octahedron is inferred to be a consequence of the lack of sensitivity of the EXAFS technique.[43] The lack of significant peaks in the Fourier transforms corresponding to higher-shell Ir–Ir neighbors is also consistent with the inference that there was no significant sintering of the Ir to form crystallites on the outer zeolite surface.

There is an analogy between the chemistry of iridium carbonyls in NaY zeolite and that of rhodium carbonyls in NaY zeolite.[51] However, the analogy has not been shown to extend to the simple decarbonylation of the clusters; the present results indicate a decarbonylation of the iridium carbonyl without loss of cluster nuclearity, but the decarbonylation of $[Rh_6(CO)_{16}]$ led to growth in cluster nuclearity, as indicated by EXAFS results.[51]

The Ir–Ir distance characterizing the decarbonylated Ir_6 clusters in NaY zeolite is 2.71 Å, which is the same as the Ir–Ir distance in bulk Ir metal.[69] The comparison is not as simple as one would wish, however, as the samples were characterized by EXAFS spectroscopy in the presence of H_2. Tzou et al.[70] reported that the Rh–Rh distance of reduced Rh clusters in NaY zeolite was about 2% shorter than that in Rh foil, but their sample had been purged with He. We expect that our reduced samples incorporated adsorbed hydrogen in the EXAFS experiment, and adsorbed hydrogen has been shown to increase the Rh–Rh distance in γ-Al_2O_3-supported Rh[71] and Y zeolite-supported Pt.[72]

In summary, these observations indicate that the structure of the Ir cluster frame after decarbonylation under mild conditions resembled that of the octahedral frame of $[Ir_6(CO)_{16}]$. The decarbonylated hexairidium clusters are inferred to be similar to those that have been inferred to form by decarbonylation of $[Ir_6(CO)_{15}]^{2-}$ supported on MgO;[43] it is possible that the clusters are stabilized by the rigid environment of the zeolite cages and migrate and sinter less rapidly than they would on a support with larger pores.

(65) Tanaka, K.; Watters, K. L.; Howe, R. F. *J. Catal.* **1982**, *75*, 23.
(66) Psaro, R.; Dossi, C.; Fusi, A.; Della Pergola, R.; Garlaschelli, L.; Roberto, D.; Sordelli, L.; Ugo, R.; Zanoni, R. *J. Chem. Soc., Faraday Trans.* **1992**, *88*, 369.
(67) Handy, B. E.; Dumesic, J. A.; Langer, S. H. *J. Catal.* **1990**, *126*, 73.
(68) Primet, M. *J. Catal.* **1984**, *88*, 273.
(69) Wyckoff, R. W. G. *Crystal Structures*, 2nd ed.; Wiley: New York, **1963**; Vol. 1, p 10.
(70) Tzou, M. S.; Teo, B. K.; Sachtler, W. M. H. *Langmuir* **1986**, *2*, 773.
(71) van't Blik, H. F. J.; van zon, J. B. A. D.; Huizinga, T.; Vis, J. C.; Koningsberger, D. C.; Prins, R. *J. Am. Chem. Soc.* **1985**, *107*, 3139.
(72) Moraweck, B.; Clugnet, G.; Renouprez, A. *Surf. Sci.* **1979**, *81*, L631.

Recarbonylation of the Decarbonylated Iridium Clusters. The results show that both isomers of $[Ir_6(CO)_{16}]$ in NaY zeolite could be decarbonylated; recarbonylation initially gave the isomer of $[Ir_6(CO)_{16}]$ with edge-bridging ligands. This could be converted to the isomer with face-bridging ligands, so that the decarbonylation–carbonylation processes were reversible.

In contrast, it has typically been found that CO adsorption leads to significant morphological changes in supported clusters of group 8 metals; the processes are usually irreversible. The details of the surface chemistry depend on the metal cluster size and hydroxyl group content of the support surface. For example, the adsorption of CO on highly dispersed clusters of Rh[71,73,74] as well as Ru[75] supported on γ-Al_2O_3 leads to the oxidative fragmentation of the clusters; the resulting surface species are metal subcarbonyls. When clusters of more noble metals (Pd[76] or Pt[77]) on metal oxide or zeolite supports are brought in contact with CO, they aggregate to form larger clusters. The surface hydroxyl groups have been suggested to play a principal role in both cases.

Thus it appears that the combination of iridium and the zeolite may be nearly unique in allowing the reversible decarbonylation and recarbonylation with retention of the cluster nuclearity. It may be that iridium is not too noble and sufficiently oxophilic to resist ready agglomeration or fragmentation, and the zeolite cages may help to stabilize the hexairidium clusters.

Experimental Section

Materials and Catalyst Synthesis. Synthesis of the zeolite-supported organometallics was performed with samples in a Braun MB-150M drybox purged with N_2 that recirculated through O_2- and moisture-scavenging traps or on a Schlenk vacuum line that was purged with N_2 (99.999%). The drybox was equipped with O_2 and moisture detectors and the concentrations of these contaminants were <1 ppm. Crystalline NaY zeolite powder (LZY-52) was supplied by Union Carbide. It had a unit cell size of 24.7 Å and a silica/alumina molar ratio of 4.74. Prior to preparation of the zeolite-supported samples, the zeolite was evacuated at 10^{-3} Torr at room temperature for 2 h, but it was not rigorously dried. $[Ir(CO)_2(acac)]$ (Strem) was used without purification. Reagent grade mixed hexanes were purged with N_2 for several hours before use as a solvent. He and H_2 (Matheson, 99.999%) were purified by passage through traps containing particles of Cu_2O and particles of activated zeolite to remove traces of O_2 and moisture, respectively. CO (Matheson, UHP grade) was purified by passage through a trap containing particles of activated alumina heated to a temperature exceeding 250 °C to remove any traces of metal carbonyls from the high-pressure gas cylinder and through a trap containing particles of activated zeolite to remove moisture.

In the preparation of the zeolite-supported Ir samples, $[Ir(CO)_2(acac)]$ (60 mg/g of zeolite) was dissolved in hexanes and brought in contact with the pre-evacuated NaY zeolite. The white zeolite powder became dark gray, and the initially greenish-black solution became clearer after being stirred for several hours. After 2 days, the slurry was black. The mixture was filtered and the zeolite washed thoroughly with hexanes and dried under vacuum at room temperature for 12 h. The weight of the residual iridium precursor, measured after evaporation of the extract solvent, indicated that the zeolite contained about 0.8 wt % of Ir. The samples were stored in the drybox.

Catalytic Hydrogenation of CO. CO hydrogenation kinetics measurements were made with a copper-lined stainless-steel tubular flow reactor having an inner diameter of $^1/_4$ in. Typically, 1.0 g of catalyst was loaded into the central (isothermal) zone of the reactor in the glovebox; the upstream and downstream reactor sections were packed with glass wool. The gases used as feeds to the reactor, CO (Matheson, UHP grade) and H_2 (Matheson, UHP grade), were passed through a trap containing particles of activated 4A zeolite; H_2 also flowed through a trap containing particles of Cu_2O to remove residual O_2. CO flowed through a trap containing particles of activated carbon at 300 °C to remove residual metal carbonyls. The reactor was first pressurized in CO + H_2 (equimolar) to 20 atm. The sample temperature was then ramped with a heating rate of 2.5 deg/min to 250 °C in flowing CO + H_2 (12 mL (NTP)/min). Time zero on stream was defined as the time when this temperature was reached. The effluent stream flowed through a heated line (ca. 140 °C) to prevent condensation of products, which were intercepted periodically for analysis in an Antek 300 gas chromatograph equipped with a flame ionization detector. The products were separated on a Porapak Q column (4 ft in length and $^1/_8$ in. in inside diameter) in a temperature-programmed mode with the column heated at a rate of 4 deg/min from 85 to 125 °C and held at 125 °C for 50 min. The C_1–C_6 hydrocarbon (alkane and alkene) as well as oxygenate (methanol, ethanol, and dimethyl ether) products were identified and quantified by use of calibration gas mixtures. Conversions (<2%) were measured as a function of time on stream for periods as long as 8 days to provide data characterizing catalyst deactivation. At the conclusion of each experiment, the catalyst was cooled at room temperature in flowing CO and H_2 (equimolar), and the pressure was decreased to 1 atm. The sample was unloaded in the drybox in preparation for further characterization.

Infrared Spectroscopy. Transmission infrared spectra of the zeolite samples were collected with a Nicolet 7199 (FTIR) spectrometer with a resolution of 4 cm^{-1}. Samples were pressed into semitransparent wafers in the drybox and mounted in the infrared cell. The experiments were performed with the samples in controlled atmospheres; purified He, N_2, CO, or H_2 (or any of these gases containing some water) could be delivered to the cell, which was part of a flow system. A typical gas flow rate was 20–30 mL (NTP)/min. Samples were scanned 32 or more times and the data averaged.

X-ray Absorption Spectroscopy. The EXAFS experiments were performed on X-ray beamline X-11A at the National Synchrotron Light Source at Brookhaven National Laboratory, Upton, Long Island, New York. The ring energy was 2.5 GeV and the ring current 80–220 mA. The spectra were recorded with the sample in a cell that allowed treatment in flowing gases prior to the measurements. The powder samples were pressed into wafers with a C-clamp inside a glovebag purged with N_2 boiloff gas from a liquid nitrogen cylinder. The amount of sample in a wafer (approximately 150 mg) was calculated to give an absorbance of 2.5 at the Ir L_{III} absorption edge. After the sample had been pressed, it was unloaded from the die and loaded into the EXAFS cell. The cell was then sealed under a positive pressure of N_2, removed from the glovebag, aligned in the X-ray beam, and cooled with liquid nitrogen. The EXAFS data were recorded in the transmission mode after the cells had been cooled with liquid nitrogen. The data were collected with a Si(111) double crystal monochromator that was detuned by 30% to minimize the effects of higher harmonics in the X-ray beam. Each sample was scanned at energies near the Ir L_{III} edge (11215 eV).

Four samples were characterized with EXAFS spectroscopy. Two samples were NaY zeolite containing the isomer of $[Ir_6(CO)_{16}]$ with face-bridging ligands prepared from $[Ir(CO)_2(acac)]$ in the zeolite in the presence of CO + H_2 (equimolar) at 20 atm and 250 °C for 1 day and for 8 days. Each of these samples was scanned twice under N_2. The third sample was prepared from the first sample treated in CO + H_2 for 1 day. After data collection with the first sample, the cell was allowed to warm to room temperature, and flow of H_2 (50–100 mL (NTP)/min) was started. The sample was then decarbonylated in flowing H_2 by heating the cell at a rate of 3 deg/min from 25 to 300 °C and holding at 300 °C for 1 h. The cell was cooled to room temperature in flowing H_2 and sealed under a positive pressure of H_2. The cell was then aligned and cooled to liquid nitrogen temperature, and the EXAFS spectrum was again measured. The fourth sample was the recarbonylated $[Ir_6(CO)_{16}]$ sample. The sample was prepared in Delaware by first decarbonylating the first EXAFS sample described above at 300 °C for 1 h in flowing H_2 at 1 atm. It was recarbonylated by treatment in flowing CO at 175 °C for 12 h. The sample was loaded into the EXAFS cell in a N_2-filled glovebag and then scanned twice at liquid nitrogen temperature in the N_2 environment.

EXAFS Reference Data. The EXAFS data were analyzed with experimentally determined reference files obtained from EXAFS data for materials of known structure. The Ir–Ir and Ir–$O_{support}$ interactions were analyzed with phase shifts and backscattering amplitudes obtained from EXAFS data for Pt foil and $Na_2Pt(OH)_6$, respectively. The transferability of the phase shift and backscattering amplitudes for Pt and Ir has been justified experimentally[78] and theoretically.[79] The Ir–C

(73) Paul, D. K.; Yates, J. T., Jr. *J. Phys. Chem.* **1991**, *95*, 1699.
(74) Ballinger, T. H.; Yates, J. T., Jr. *J. Phys. Chem.* **1991**, *95*, 1694.
(75) Solymosi, F.; Rasko, J. *J. Catal.* **1989**, *115*, 107.
(76) Zhang, Z.; Chen, H.; Sheu, L.-K.; Sachtler, W. M. H. *J. Catal.* **1991**, *127*, 213.
(77) Chang, J.-R.; Koningsberger, D. C.; Gates, B. C. *J. Am. Chem. Soc.* **1992**, *114*, 6460.
(78) Duivenvoorden, F. B. M.; Koningsberger, D. C.; Uh, Y. S.; Gates, B. C. *J. Am. Chem. Soc.* **1986**, *108*, 6254.

Table V. Crystallographic Data Characterizing the Reference Compounds and Fourier Transform Ranges Used in the EXAFS Analysis[a]

	crystallographic data			Fourier transform		
sample	shell	N	R, Å	Δk, Å^{-1}	Δr, Å	n
Pt foil	Pt–Pt[b]	12	2.77	1.9–19.8	1.9–3.0	3
$Na_2Pt(OH)_6$	Pt–O[c]	6	2.05	1.4–17.7	0.5–2.0	3
$[Ir_4(CO)_{12}]$	Ir–C[d]	3	1.87	2.8–16.5	1.1–2.0	3
	Ir–O* [d]	3	3.01	2.8–16.5	2.0–3.3	3

[a] Notation as in Table I; Δk, limits used for forward Fourier transformation (k is the wave vector); Δr, limits used for shell isolation (r is distance); n, power of k used for Fourier transformation. [b] Crystal structure data from ref 69. [c] Crystal structure data from ref 81. [d] Crystal structure data from ref 82; after subtraction of the Ir–Ir contribution: $N = 6$, $R = 2.69$ Å, $\Delta\sigma^2 = -0.001$ Å^2, and $\Delta E_0 = 2.5$ eV.

and Ir–O* interactions were analyzed with phase shifts and backscattering amplitudes obtained from EXAFS data for crystalline $[Ir_4(CO)_{12}]$ (which has only terminal CO ligands) mixed with SiO_2. $[Ir_4(CO)_{12}]$ was chosen because the multiple scattering effect in the Ir–O* shell is significant as a consequence of the linearity of the Ir–C–O moiety, and it was necessary to fit with a reference that exhibits multiple scattering.[80] The details of the preparation of the reference files are described elsewhere,[28] and the parameters used to extract these files from the EXAFS data are summarized in Table V.

Conclusions

$[Ir(CO)_2(acac)]$ in the cages of NaY zeolite was converted in CO at 1 atm to the isomer of $[Ir_6(CO)_{16}]$ with edge-bridging ligands and in CO + H_2 at 20 atm to the isomer of $[Ir_6(CO)_{16}]$ with face-bridging ligands, either of which could be reversibly decarbonylated. The latter clusters are the predominant iridium-containing species in catalysts for CO hydrogenation giving high selectivity for propane. EXAFS spectra characterizing the iridium clusters are consistent with the inference that most of the clusters maintained the octahedral metal framework of $[Ir_6(CO)_{16}]$, even after decarbonylation. These results illustrate the potential for preparation of supported metal clusters with controlled nuclearities and open the door for precise characterization of the structures and properties of uniform, highly dispersed supported metal catalysts.

Acknowledgment. We thank Professor D. C. Koningsberger of the University of Utrecht for many helpful discussions about EXAFS analysis. The EXAFS data were analyzed with the Eindhoven University EXAFS Data Analysis Program, developed by M. Vaarkamp and D. C. Koningsberger. We thank Dr. Edith Flanigen of Union Carbide Corp. for providing the sample of NaY zeolite. This research was supported by the National Science Foundation (CTS-9012910). We also acknowledge the support of the U.S. Department of Energy, Division of Materials Sciences, under Contract No. DE-FG05-89ER45384, for its role in the operation and development of beam line X-11A at the National Synchrotron Light Source. The NSLS is supported by the Department of Energy, Division of Materials Sciences and Division of Chemical Sciences, under Contract No. DE-AC02-76CH00016. We are grateful to the staff of beam line X-11A for their assistance.

(79) Teo, B.-K.; Lee, P. A. *J. Am. Chem. Soc.* **1979**, *101*, 2815.
(80) Teo, B.-K. *J. Am. Chem. Soc.* **1981**, *103*, 3990.
(81) Tromel, M.; Lupprich, E. *Z. Anorg. Chem.* **1975**, *414*, 160.
(82) Churchill, M. R.; Hutchinson, J. P. *Inorg. Chem.* **1978**, *17*, 3528.